Analysis of lifting operation of a monopile for an offshore wind turbine considering vessel shielding effects*

Lin Li †[1,2], Zhen Gao[1,2], Torgeir Moan[1,2] and Harald Ormberg[3]

[1]Centre for Ships and Ocean Structures (CeSOS), NTNU, Trondheim, Norway

[2]Centre for Autonomous Marine Operations and Systems (AMOS), NTNU, Trondheim, Norway

[3]Norwegian Marine Technology Research Institute (MARINTEK), Trondheim, Norway

Abstract

This study addresses numerical simulations of the lifting operation of a monopile for an offshore wind turbine with a focus on the lowering process. A numerical model of the coupled system of the monopile and vessel is established. The disturbed wave field near the vessel is investigated and observed to be affected by the diffraction and radiation of the vessel. The shielding effects of the vessel during the continuous lowering operation are accounted for in this study by developing an external Dynamic Link Library (DLL) that interacts with SIMO program in the time-domain simulations. The DLL is implemented by interpolating fluid kinematics between pre-defined wave points near the vessel. Based on the time-domain simulations, the critical responses, such as the motions of the monopile, the tensions in the lift wire and the contact forces in the gripper device in the disturbed wave fields, are compared with those in incident wave conditions. The results indicate that a great reduction in these extreme responses can be achieved when the shielding effects are considered. The sensitivity study of the responses in different wave directions is performed. The results indicate different behaviours with different wave directions and with short or long waves. A comparison of the responses when using a floating vessel and a jack-up vessel is also studied and can be used to support the choice of installation vessel type.

Keywords: lifting operation, shielding effect, monopile, time-domain simulation

*Prof. Jøgen Juncher Jensen serves as editor for this article.

† lin.li@ntnu.no, tlf: +47 73 55 11 12, fax: +47 73 59 55 28

1 INTRODUCTION

Various support structures have been proposed for offshore wind turbines (OWTs) at different water depths and soil conditions. With bottom-fixed OWTs, the industry prefers working with four types of foundations: gravity-based, monopile, jacket and tripod [1]. Of these foundations, monopiles are the most commonly used foundations in water depths up to 40 metres, and it is estimated that more than 75% of all installations are founded on monopiles [2]. A typical monopile is a long tube with a diameter of 4 to 6 metres. It is driven into the sea bed using a large hydraulic hammer if the soil condition is suitable. The pile diameter is limited by the size of the available driving equipment.

The installation of a monopile generally includes the following steps:

1. Upending the monopile from a horizontal position on the vessel to a vertical position.

2. Lowering the monopile down through the wave zone to the sea bed. The hydrodynamic wave loads induce the motions of the monopile when it passes through the wave zone. The monopile should be precisely landed at the designated point on the sea bed.

3. Driving the monopile into the sea bed with a hydraulic hammer.

This study focuses on the second step, i.e. the process of lowering the monopile.

Lifting operations are the most common means of installing monopiles and of many other offshore structures. Numerical studies have been commonly used to estimate the response characteristics of offshore lifting operations, including the installation of sub-sea templates [3], suction anchors [4], foundations and topsides of platforms, wind turbine components [5] and so on. A few experimental studies have also been conducted to obtain accurate hydrodynamic coefficients, e.g., the hydrodynamic mass and damping of ventilated piles [6], or to tune the critical parameters for numerical models, e.g., the damping or stiffness level of important support structures in the lifting system [7].

In lifting operations with objects (e.g., monopiles) lowered from air into the splash zone and towards the sea bed, the dynamic features of the system change continuously. A process dominated by transient or highly non-linear responses must be analysed differently from a stationary case. There are generally two approaches to simulate such cases [8]:

1. Find the most critical vertical position of the object by simulating a lowering in harmonic waves, and then make steady state simulations in irregular waves at this position.

2. Simulate a repeated lowering with different irregular wave realizations, and study the extreme response observed in each simulation.

It was demonstrated that the second method provides more realistic results [8]. The reason is that an unrealistic build-up of the oscillations that are observed in stationary cases is avoided. Therefore, to provide more accurate estimates of the operations, analyses of the entire lowering process are required.

In lifting operations conducted by floating vessels, hydrodynamic interactions between the structures in waves are of great importance. Studies have been performed to investigate the heavy lifting operations in the oil and gas industry considering shielding effects, such as the lifting of a heavy load from a transport barge using a large capacity semi-submersible crane vessel [9], [10], [11]. The studies found that the hydrodynamic interaction had little effect on the responses of the crane tip, but affected the responses of the transport barge and thus greatly affected the lifting operations because of the small dimension of the barge compared with that of the crane vessel [11]. Therefore, the hydrodynamic interaction between two floaters close to each other should be taken into consideration when estimating responses.

In the case of lifting a monopile using a floating vessel, due to the small dimension of the monopile compared with the vessel, the hydrodynamic effects of the monopile on the vessel are minor and can be ignored. However, the shielding effects of the vessel are expected to have a large influence on the responses of the monopile. The wave fields near the floating vessel are altered from the original incident waves, and three-dimensional effects would occur due to the diffraction and radiation from the vessel even if the incident wave is long-crested. If the lifting system and the vessel are placed in proper positions relative to the incident waves, the responses of the lifting system in waves can be less than those if the lifting system is exposed in the incident waves because of the wave shadow effects. Thus, it is crucial to study the vessel shielding effects when conducting lowering operations through waves in the vicinity of the vessel.

According to DNV-RP-C205 [12], with small structures close to a floater of large volume, the radiation and diffraction effects on fluid kinematics should be considered when calculating the forces on the structure. To account for those effects, the typical approach is to obtain the transfer functions of the fluid kinematics at the position of the operation near the floating vessel in the frequency domain and then to calculate the forces on the lifted object using the fluid kinematics obtained from the transfer functions. This approach is only valid when the lifting system is in a stationary position, i.e., when it has a stationary mean position. However, as discussed above, due to transients and the non-linearity of the system, the entire lowering process should be conducted with time-varying positions of the lifted objects. Therefore, time-domain methods to estimate the entire lowering process while considering the shielding

effects by the vessel are required.

The current work focuses on the lowering phase of the installation of a monopile foundation with consideration of the shielding effects of the vessel. The fluid kinematics near the installation vessel were studied first. Time-domain simulations were performed using multi-body code SIMO [13]. The wave forces on the monopile during lowering were calculated using an external Dynamic Link Library (DLL) that included the shielding effects from the installation vessel. The responses of the lifting system in disturbed wave fields were quantified and compared with the responses in undisturbed incident waves. The simulation model and the methodology are presented first, followed by discussions of the results. Finally, conclusions and recommendations are given to guide future lifting operations with regards to issues of shielding effects.

2 MODELLING OF THE LIFTING SYSTEM

2.1 Model description

A floating installation vessel was chosen for the monopile installation. The main dimensions of the vessel are presented in Table 1. The vessel was a monohull heavy lift vessel. The crane was capable of performing lifts of up to 5000 tons at an outreach of 32 metres in fully revolving mode. The main hook featured a clear height to the main deck of the vessel of maximum 100 metres. The vessel had been designed with a combination dynamic positioning system and eight-line mooring system. The positioning system allowed the operations of the vessel in shallow water and in close proximity to other structures. Therefore, the lifting capacity and the positioning system of the floating vessel made it capable of performing the installation of monopiles in shallow-water sites. The monopile used in the model was a long slender hollow cylinder with main dimensions listed in Table 1.

Fig. 1 shows a schematic layout of the arrangement of the operation. The system included two rigid bodies, i.e., the floating installation vessel and the monopile. A hook is generally used to connect the lift wire and the sling that attached the monopile. In the current model, the sling was assumed to be very stiff. Hence, the hook and the monopile were considered to be rigidly connected and were modelled as one body for simplicity.

The dynamic responses of a floating crane and a heavy load with a flexible boom were studied in [14] by modelling the crane boom using finite element method (FEM). The dynamic factor analysis showed a difference of less than 5% between the elastic boom and the rigid boom in their study. It was also shown

that the influence of the elastic boom decreased significantly with the decrease of the load mass. In their study, the maximum lifting capacity of the crane was 3600 tons and the load considered was above 1300 tons, more than 30% of the crane capacity. By comparison, the monopile mass is around 10% of the crane capacity in the current study. Thus, the effect of the elasticity of the crane boom is negligible. The crane was rigidly connected to the vessel in the numerical model, and a low constant flexibility of the crane was included.

The global coordinate system was a right-handed coordinate system with the following orientation: the X axis pointed towards the bow, the Y axis pointed towards the port side, and the Z axis pointed upwards. The origin was located at [mid-ship section, centre line, still-water line] when the vessel was at rest. The positions of the crane tip and the monopile were chosen based on practical operations.

Two types of couplings between the vessel and the monopile were included in the numerical model: the wire coupling through the main lift wire and the coupling via the gripper device. The lift wire started at the bottom of the crane where a winch was located; thus, the lift wire could be extended through the winch to lower the monopile. The function of the gripper device was to control the horizontal motions of the monopile during lowering and landing as well as to support the monopile during driving operations. The gripper device was also rigidly fixed to the vessel.

2.2 Coupled equations of motion

The two-body coupled lifting system included 12 degrees of freedom (DOFs) of rigid body motions. The 12 equations of motion are given in Eqn. 1.

$$(\mathbf{M} + \mathbf{A}(\infty)) \cdot \ddot{\mathbf{x}} + \mathbf{D_1}\dot{\mathbf{x}} + \mathbf{D_2} f(\dot{\mathbf{x}}) + \mathbf{K}\mathbf{x} + \int_0^t \mathbf{h}(t-\tau)\dot{\mathbf{x}}(\tau)d\tau = \mathbf{q}(t, \mathbf{x}, \dot{\mathbf{x}}) \tag{1}$$

where,

$\mathbf{M}$ the total mass matrix of the vessel and the monopile;

$\mathbf{x}$ the rigid-body motion vector with 12 DOFs;

$\mathbf{A}$ the frequency-dependent added mass matrix;

$\mathbf{D_1}$ the linear damping matrix;

$\mathbf{D_2}$ the quadratic damping matrix;

$\mathbf{K}$ the coupled hydrostatic stiffness matrix;

$\mathbf{h}$ the retardation function of the vessel, which is calculated from the frequency-dependent added

mass or potential damping;

$\mathbf{q}$ the external force vector that includes the wind force q_{WI}, the 1st and 2nd order wave excitation forces $\mathbf{q}^{(1)}{}_{WA}$ and $\mathbf{q}^{(2)}{}_{WA}$, the current force $\mathbf{q}_{CU}$ and any other external forces $\mathbf{q}_{EXT}$.

The coupled stiffness matrix $\mathbf{K}$ includes the hydrostatic stiffness of the vessel, the stiffness from the mooring line, and the coupling between the vessel and the monopile via the lift wire and gripper device.

2.3 Modelling of the vessel and the monopile

The potential added mass and damping coefficients, the hydrostatic stiffness and the first order wave excitation force transfer functions were calculated in WADAM based on the panel method [15], and then the retardation functions in Eqn. 1 and the 1st order excitation force were obtained. In the current vessel model, the following simplifications were applied:

1. Waves were considered as main factor, and wind and current forces were not included.

2. The exciting forces on the floating vessel in the model consisted of only the 1st order wave excitation force vector $\mathbf{q}^{(1)}{}_{WA}$, and no 2nd order wave forces were included as shielding effects are only relevant in the wave frequency range.

3. The mooring line system was simplified into linear stiffness terms in surge, sway and yaw. The viscous effects from the vessel hull and the mooring system were simplified into linear damping terms in surge, sway and yaw. The roll damping of the vessel was also included.

The external forces on the monopile included the gravity force, the buoyancy force, as well as the hydrodynamic wave forces. Because the structure was a hollow steel cylinder of low thickness, the wave forces acting on the bottom of the monopile were negligible. The main contributions, therefore, were the wave forces normal to the monopile's central axis.

In an operational sea state, the diameter of the monopile is relatively small compared with the wave length, and the ratio of wave height to structure diameter is low. According to the wave force regimes in [12], the inertial force is the governing force on the monopile. Furthermore, the motion of the monopile is large and the submergence increases during the lowering phase; thus, the linear theory from the panel method based on a mean position is not applicable. The instantaneous position of the monopile must be considered at each time step. Thus, Morison's formula should be used, and the monopile should be simulated as a slender body using strip theory. The horizontal wave force $f_{W,s}$ per unit length on each strip of a vertical moving circular cylinder can be determined using Morison's equation [16].

$$f_{w,s} = \rho_w C_M \frac{\pi D^2}{4} \cdot \ddot{\zeta}_s - \rho_w C_A \frac{\pi D^2}{4} \cdot \ddot{x}_s + \frac{1}{2} \rho_w C_q D \left| \dot{\zeta}_s - \dot{x}_s \right| \cdot (\dot{\zeta}_s - \dot{x}_s) \tag{2}$$

In this equation, the positive force direction is the wave propagation direction. $\ddot{\zeta}_s$ and $\dot{\zeta}_s$ are fluid particle acceleration and velocity at the centre of the strip, respectively; $\ddot{x}_s$ and $\ddot{x}_s$ are the acceleration and velocity at the centre of the strip due to the body motions; D is the outer diameter of the cylinder; and C_M, C_A and C_q are the mass, added mass and quadratic drag force coefficients, respectively.

The first term in the equation is the wave excitation force, including diffraction and Froude-Krylov force (FK term). The second term is the inertial term and the third term is the quadratic drag term. C_M and C_q are dependent on many parameters, such as the Reynolds number (Re), the Kaulegan-Carpenter number (KC) and the surface roughness ratio [16]. The outer surface of the monopile was assumed to be smooth, and Re number had a magnitude of 10^6 to 10^7. The KC number in the operational sea states was in the range of 1 to 3. According to [12], the quadratic drag coefficient can be chosen as $C_q = 0.7$, which takes into account the flow separation of the water outside of the monopile.

The monopile was a bottomless cylinder that partly filled with water as it was lowered. This water influenced the hydrodynamic coefficients of the cylinder. Moreover, the submerged length of the cylinder increased with time. Several numerical studies have been conducted to estimate the hydrodynamic coefficients and excitation forces on bottomless cylinders with finite wall thickness, and the results showed a great dependency of these parameters on the wall thickness and the submergence of the cylinder [17], [18], [19]. Therefore, it is necessary to investigate the hydrodynamic coefficients of the bottomless monopile considering different submergences. The added mass coefficients of the monopile at different submergences were calculated using WADAM [15]. The results were three-dimensional ($3D$) hydrodynamic added mass of the whole body. However, in order to use strip theory to simulate the hydrodynamic forces in SIMO, $2D$ coefficients are required. Hence, the $2D$ added mass coefficients were obtained by dividing the $3D$ coefficients by the submerged length.

Fig. 2 shows the non-dimensional $2D$ added mass coefficients in transverse directions at different submergence. The figure shows that the $2D$ added mass coefficients increase with submerged length. However, at submergences of greater than 5 metres, the non-dimensional $2D$ added mass coefficients approach to a constant of approximately 1.8 at the wave frequencies considered. Furthermore, the total excitation forces calculated using Morison's equation and strip theory with the $2D$ added mass coefficients were compared with the $3D$ excitation forces calculated directly using WADAM. Good agreement was

obtained at submergences larger than 5 metres. Because the response at submergence of less than 5 metres is not as critical as at greater submergences, an asymptotic value of $C_M = C_A = 1.8$ was chosen as the $2D$ added mass coefficient in Eqn. 2. Thus, forces at each strip can be obtained and then integrated along the submerged part to obtain the total force and moment. It was also confirmed that the resonant flow motions (sloshing) inside the monopile did not occur at the wave frequencies of interest. Moreover, in the simplified $2D$ model the effects of water exchange and flow separation at the end of the monopile were not considered.

The water depth at the installation site is 25 metres, and the significant wave height for performing such lifting operations is normally below 2.5 metres. According to the ranges of validity for various wave theories [12], the wave conditions considered in the numerical study are near the boundary of the 1st order linear waves and the 2nd order waves. The non-linearities in waves and the fluctuating wave elevation in shallow water depth will induce the high-frequency components in wave load and result in larger responses of the structure [20]. These are relevant in predicting extreme loads on the monopile in severe conditions during its operational phase. However, as the installation phase is very transient and the sea states are low, the effects of the non-linearities in waves on the lifting system are expected to be very small and the linear wave theory is used for calculating the wave forces in the current model.

2.4 Mechanical couplings

The coupling between the on-board crane and the monopile was achieved using a lift wire. The wire coupling force was modelled as a linear spring force according to the following equation [13]:

$$T = k \cdot \Delta l \tag{3}$$

where T is the wire tension, Δl is the wire elongation and k is the effective axial stiffness, which is given by:

$$\frac{1}{k} = \frac{l}{EA} + \frac{1}{k_0} \tag{4}$$

where E is the modulus of elasticity, A is the cross-sectional area of the wire, $1/k_0$ is the crane flexibility and l is the total length of the wire, which increases as the winch runs during the lowering operation.

From the positions of the two ends of the wire, the elongation and thereby the tension can be determined. The material damping in the wire was included in the model.

The physical model of the gripper device is normally a ring-shaped structure with several contact elements in the inner circumference which behave like bumpers during installation (see section view Fig. 3 (a)). Thus, the gripper force in the numerical model was simplified by a spring-damper system. The gripper device was modelled as a contact point attached to the vessel. A cylinder fixed to the monopile with a vertical axis was modelled at the same time, and the contact point was placed inside the cylinder (see Fig. 3 (b)). When the monopile tends to move away from the gripper, the contacts between the cylinder and the contact point will provide restoring and damping forces for the monopile and control its horizontal motions. With the lowering of the monopile, the contact force always occurs at the gripper position which corresponds to the contact point in the numerical model. Rotation symmetric stiffness and damping around the axis were assumed and were defined by specifying restoring and damping forces F_i at several relative distances Δd_i between the contact point and the cylinder axis. An interpolation was used for all the other relative distances and the gripper forces at each time instance can be obtained. The physical and numerical models for the gripper coupling are illustrated in Fig. 3. Sensitivity studies to quantify the effects of the gripper stiffness on the responses during the lowering of a monopile were performed in [21]. The study showed that the gripper contact force and the relative motion between the monopile and the gripper device were very sensitive to the gripper stiffness, while the influence on the monopile rotational motion and lift wire tension were minor. In the current study, a representative gripper device stiffness was used for all the simulations.

The properties of the lift wire and the gripper device are presented in Table 2.

2.5 Eigen value analysis

The eigen value analysis was conducted in the frequency domain to investigate the eigen periods of the rigid body motions of the lifting system. The natural modes and natural periods were obtained by solving Eqn. 5.

$$[-\omega^2(\mathbf{M}+\mathbf{A})+\mathbf{K}]\cdot\mathbf{x}=0 \tag{5}$$

where $\mathbf{M}$ is the mass matrix of the vessel and the monopile. $\mathbf{A}$ is the added mass matrix; for the vessel the added mass with infinite frequency was used. $\mathbf{K}$ is the total restoring stiffness matrix, which is split into three contributions: hydrostatic restoring, mooring restoring and coupling between the vessel and the monopile. The coupling restoring includes the wire coupling and the gripper device coupling. $\mathbf{x}$ is the eigen vector that represents rigid-body motions with 12 DOFs in the two-body coupled system and

6 DOFs if a single body is considered. The eigen values of the vessel alone and of the monopile alone were studied as well as the eigen values of the coupled system.

The natural periods and natural modes of the vessel and of the monopile are listed in Table 3 and Table 4, in which the dominated rigid motions are emphasised. The natural periods of the heave, pitch and roll motions of the vessel indicate small motions in short waves and larger motions when the wave period is close to the natural periods. In lifting operations, the motions of the vessel affect the motions of the monopile through the lift wire and the gripper device, the motions of which in three directions are formulated in Eqn. 6:

$$\mathbf{s} = (\eta_1 + z\eta_5 - y\eta_6)\hat{i} + (\eta_2 - z\eta_4 + x\eta_6)\hat{j} + (\eta_3 + y\eta_4 - x\eta_5)\hat{k} \tag{6}$$

where η_1 to η_6 are the rigid body motions of the vessel and (x, y, z) is the position of the crane tip or gripper relative to the fixed coordinates of the vessel body. It is expected that the vessel motions will play an important role in the response of the monopile when the wave periods are approximately $T_p = 9$ sec to 14 sec.

In the case of the monopile by itself, the vessel was assumed to be a fixed structure and the lift wire and the gripper provided the restoring force for the monopile; the natural periods of the monopile in Table 4 correspond to the initial position of the monopile in air before being lowered and the eigenvectors refer to the monopile body-fixed coordinate with the origin at the center of the monopile (see Fig. 4). The 1st mode is dominated by the heave motion of the monopile, and the stiffness in heave is mainly from the lift wire axial stiffness. Modes 2 to 5 are dominated by a combination of the rotational motion in vertical plane and the translational motion in the horizontal plane, and the last mode is pure yaw motion. The eigenvectors in Table 4 show that modes 2 and 3 are symmetric and correspond to the same eigenperiods, but occur in different planes. It is the same for mode 4 and 5. The mode shapes are illustrated in Fig. 4, where the eigenvectors from Table 4 are magnified by a factor of 10. The eigenmodes are shown in different planes in order to observe the differences. The eigenperiods for modes 4 and 5 are much longer than modes 2 and 3. This can be explained as follows: both the translations and the rotations in mode 2 and 3 tend to increase the relative displacement between the monopile and the gripper. In this case, the gripper should provide enough restoring force to force the monopile move back to its initial position. On the other hand, the rotations and translations in modes 4 and 5 counteract each other and result in less displacement of the monopile relative to the gripper. The restoring provided by the gripper is then

reduced compared with the previous case and results in longer eigenperiods. This can also be observed from the eigenmodes in Fig. 4.

In the coupled system of the vessel and the monopile, it is difficult to interpret the twelve eigen modes because of the coupling effects. However, it was observed that in general the motions of the vessel slightly decreased the natural periods of the rotational modes of the monopile, and the natural period of the vessel roll motion was also reduced due to the effect from the lifting system.

During the installation, the position of the monopile changes with the running winch. This results in changes in the total restoring force due to changes in the length of the lift wire and in the gripper position relative to the centre of the pile. Additionally, the added mass matrix increases due to the increasing submergence. Fig. 5 shows how the eigen periods of modes 1 to 5 varied depending on the vertical position of the lower end of the monopile. The wave spectra are also included to show the modes that dominated the response at different sea states. The natural periods of mode 1 (which is heave dominated) decreased slightly with increasing submergence due to the increase in the length of the lift wire. The other four modes all increased greatly due to significant contributions from the added mass.

For wave spectra with a peak period T_p greater than 5 *sec*, there is little wave power near the natural period of the first three modes. However, modes 4 and 5 could be excited and dominate the responses at $T_p = 5$ *sec* and $T_p = 6$ *sec*, especially at a large submergence. With increasing T_p, the power of the wave spectra moves away from the natural periods of the monopile, and thus the resonance motions of the monopile would be reduced. Note that all the natural periods shown here are undamped periods and hence would increase slightly if damping were included.

3 MODELLING OF THE SHIELDING EFFECTS

The wave field around the floating vessel is different from incident wave field due to the presence and the motions of the vessel. The linear wave potential theory splits the total velocity potential into the radiation and diffraction components given by [22]:

$$\phi = \phi_D + \phi_R = \phi_I + \phi_S + \phi_R \tag{7}$$

where ϕ_D is the diffraction potential and ϕ_R is the radiation potential. ϕ_D can be further broken down into the sum of the incident velocity potential ϕ_I and the scattering velocity potential ϕ_S, which represents the disturbance to the incident wave caused by the presence of the body in its fixed position. By applying

boundary conditions, i.e., the free surface condition, the seabed condition, the body surface condition and the far field condition, the boundary value problem can be solved by numerical methods such as the panel method in the frequency domain. Thus, the hydrodynamic coefficients of the vessel and the fluid kinematics at any point in the wave field in the frequency domain can be acquired. The waves affected by both radiation and diffraction of the vessel are defined as *disturbed waves* in this paper which account for the vessel shielding effects, and the undisturbed waves are defined as *incident waves*.

To calculate the wave forces on the monopile in the disturbed wave field during lowering, the fluid kinematics $\ddot{\zeta}_s$ and $\dot{\zeta}_s$ in Eqn. 2 should be based on the disturbed fluid kinematics. Because the position of the monopile varies with time and with the increasing length of the lift wire, the fluid kinematics at each strip of the monopile are time- and position-dependent. Therefore, the following approach was chosen to simulate the lowering process of the multi-body system in the time domain while considering the shielding effects:

1. First, generate time series of disturbed fluid kinematics at pre-defined *wave points* in space. The boundary of the wave points should cover all possible positions of the wet part of the monopile during the entire lowering process.

   Calculate the disturbed fluid kinematics time series, i.e., wave elevation, velocities and accelerations at pre-defined wave points, using the fluid kinematics transfer functions in the frequency domain that are obtained using WADAM. The transfer function expresses the amplitude ratio and the phase angle between the disturbed fluid kinematics and regular incident wave amplitude. Knowing incident wave realisation $x(t)$, the Fourier transform of the kinematics of the disturbed wave $Y(\omega)$ can be calculated in the frequency domain based on $X(\omega)$, the Fourier transform of $x(t)$, and the disturbed fluid kinematics transfer functions $H(\omega)$, i.e., Eqn. 8. Thus, using inverse Fourier transform of $Y(\omega)$, the time series of wave elevations, fluid particle velocities and accelerations in disturbed waves at each pre-defined wave point can be obtained before the time-domain simulations.

$$Y(\omega) = H(\omega) \cdot X(\omega) \tag{8}$$

2. Then, at each time step of the simulation, determine the instantaneous position of the monopile based on the solutions from the previous time step. For each strip on the monopile, find the closest pre-defined wave points by comparing the coordinates of each strip on the monopile and the pre-defined wave points. By applying a $3D$ linear interpolation between these closest wave points,

the kinematics (elevations, fluid velocities and accelerations) at the centre of each strip in disturbed waves are achieved. The interpolation of the fluid kinematics is illustrated in Fig. 6.

3. Obtain the forces at each strip in disturbed waves using Eqn. 2 and then integrate along the submerged part of the monopile to acquire the total wave forces and moments on the structure. Note that due to the running winch and the motions of the monopile itself, the wet length of the monopile changes with time. The wave elevation also affects the submergence of the monopile. Therefore, it is necessary to integrate the forces up to the instantaneous wave elevation to account for non-linear force components. The instantaneous wave elevation can also be determined by an interpolation of the wave elevations at pre-defined points given the instantaneous position of the monopile.

4. Finally, perform the time-domain simulations of the coupled vessel-monopile system in irregular waves using the multi-body code SIMO and an external DLL that interacts with SIMO at each time step. SIMO calculates the wave excitation forces on the vessel and the coupling forces between the vessel and the monopile. The wave forces on the monopile in disturbed waves are calculated in DLL using the interpolation method described above, and the total wave forces on the monopile are returned to SIMO, with which the motions of the coupled system are solved. The time-domain simulation approach is illustrated in Fig. 7.

4 FLUID KINEMATICS IN THE DISTURBED WAVE FIELD

Fig. 8 shows the response amplitude operator (RAO) of wave elevation, fluid particle velocities and accelerations as a function of frequency with wave directions of 0 deg and 45 deg.

The RAOs that are given refer to the pre-defined wave points at the mean free surface when the monopile was at rest with coordinates of (-20 m, 30 m, 0 m) in the global coordinate system. The RAOs of fluid kinematics in incident waves are shown for comparison.

In long waves (with $\omega < 0.4\ rad/s$), the RAOs in disturbed waves are nearly identical to those in incident waves, which indicates that the diffraction and radiation of the vessel are negligible in long-wave conditions. However, as the frequency increases, the RAOs in disturbed waves deviate from those in incident waves, and the difference increases with frequency. When the wave length is shorter than the dimension of the vessel (approximately $\omega > 1.0\ rad/s$), the RAOs in disturbed waves are much lower than those in incident waves (with the exception of the Y-velocity at $Dir = 0\ deg$), mainly due to the

diffraction of the vessel while the radiation is minor in short waves. At a frequency near $\omega = 0.5\ rad/s$, the RAOs shift away from the main trend of the curve due to the large resonance motions of the vessel, which occur close to the natural frequencies of the vessel motions. With an increase in the frequency, the effects of the diffraction of the vessel dominate the RAOs.

The RAOs also depend greatly on the wave directions. Comparing the RAOs in Fig. 8 at 0 deg and 45 deg shows that larger discrepancies in the fluid kinematics of the two wave fields occur at 45 deg. Additionally, when $Dir = 0\ deg$, the fluid particle velocity in Y direction is not zero as it is in incident waves, which indicates the presence of $3D$ effects from the diffraction and radiation that could induce extra wave forces on the monopile in the direction perpendicular to that of long-crested incident waves.

Fig. 9 shows the variations in the fluid kinematics in all wave directions. The results in the figures, which also refer to point (-20 m, 30 m, 0 m), include four representative wave frequencies that cover long and short waves. Although the RAOs in disturbed waves are very close to those in incident waves in all wave directions in long waves, in short waves the results change considerably with direction. In general, the RAOs are reduced when the waves come from the leeward side relative to the vessel and may greatly increase when the waves come from the windward side. It is noticed that the RAOs of wave elevation and kinematics in X direction are amplified at wave directions that are larger than 180 deg in short waves, whereas the kinematics in Y direction decrease at $T_p = 7\ sec$. In fact, the fluid kinematics in the disturbed wave field are also sensitive to the position of the monopile relative to the vessel and the wave length, and cancellations may occur if this position is close to the nodes of the disturbed fluid kinematics profile. When the waves come from the leeward side, a great reduction in the RAOs occurs due to the vessel shielding effects, which results in a reduction of wave forces on the monopile during installation. Therefore, operations should be performed on the leeward side of the vessel in order to minimise the responses.

The variations in the fluid kinematics at the heading angle of 45 deg with respect to depth and to the horizontal position near the monopile installation region are shown in Figs. 10 and 11. The results in Figs. 10 correspond to points at (x = -20 m, y = 30 m) with varying depth, and the results in Fig. 11 correspond to points at the mean free surface ($z = 0\ m$) with varying X and Y positions.

As previously observed, in long waves the RAOs in disturbed waves are close to those in incident waves. Moreover, in long waves the RAOs of the fluid kinematics decay very slowly and vary little in the horizontal plane compared with those in short waves. $3D$ effects are observed in short waves along the horizontal plane as shown in Fig. 11, in which the contours of the elevation RAOs do not follow the

incident wave direction of 45 deg. The $3D$ effects are also present in Fig. 10, e.g., at $T_p = 7$ and 9 sec, at which the fluid particle velocities do not follow the decay rate as those in incident waves at depth of less than -10 m. The $3D$ effects come from the diffraction and radiation of the vessel; thus, the effects would vary from vessel to vessel. To account for the $3D$ effects when calculating the wave forces on the monopile, a $3D$ interpolation of the fluid kinematics is required.

5 TIME-DOMAIN SIMULATIONS

5.1 Time-domain simulation method

Step-by-step integration methods were applied to calculate the responses of the lifting system using an iterative routine. The equations of motion were solved by Newmark-beta numerical integration ($\beta = 0.1667$, $\alpha = 0.50$) with a time step of 0.01 sec. The 1st order wave forces of the vessel were pre-generated using Fast Fourier Transformation (FFT) at the mean position. The fluid particle motions used to calculate the hydrodynamic forces on the monopile were calculated in the time domain using the interpolation of the pre-generated fluid kinematics at pre-defined wave points in disturbed waves. The winch started at 300 sec to avoid initial transient effects with a constant speed of 0.05 m/sec, and stopped at 700 sec. Thus, the total lowering length was 20 metres. During the lowering process, the gripper device provided horizontal forces to the monopile.

The environmental condition of the time-domain simulations was $H_s = 2.5$ m. The wave spectral peak period (T_p) varied from 5 sec to 12 sec, thus covering a realistic range. At each combination of H_s and T_p the irregular waves were modelled by JONSWAP spectrum [12]. In order to account for the variability of stochastic waves, 20 realisations of irregular waves were generated at each of the environmental conditions using different seeds. Thus, 20 repetitions of the lowering simulations (400 sec for each seed) corresponded to an operation with a duration of approximately two hours.

5.2 Sensitivity study on the resolution of the pre-defined wave points

The response of the lifting system with varying resolutions of the pre-generated wave points was studied. As mentioned, the fluid kinematics at pre-defined wave points were generated based on linear wave theory, whereas those at other locations in space were obtained using a $3D$ linear interpolation. Theoretically, when a higher resolution is used, more accurate responses can be estimated. If a low resolution is chosen, the number of wave points might not be sufficient to represent the variation of the fluid kinematics in

space, which would result in a large uncertainty in the simulation results. However, a high resolution of wave points results in a large number of points at which the fluid kinematics must be pre-generated, and therefore the efficiency of the interpolation is reduced; a high resolution increases the simulation time significantly. Therefore, a reasonable resolution of wave points should be determined to provide results with an acceptable level of accuracy while at the same time shortening the simulation time.

The wave points spread in all three directions in space. The sensitivity studies in the horizontal (XY) plane and in the vertical (Z) direction were performed separately. The gaps between points in the three directions were chosen as the parameters in the sensitivity study (see Fig. 12). The parameters of the different cases are listed in Table 5. The gaps in Z direction were fixed, and all points were evenly spaced when studying the different horizontal resolutions. In the sensitivity study in the vertical direction, all the wave points were chosen at a fixed (x_0 ,y_0) position, and only one-dimensional interpolation in Z direction was used when calculating the wave forces on the monopile. A hybrid case (case 6) was included that had gaps of 0.5 metres when the depth larger than -2 m and gaps of 2 metres when the depth was less than -2 m. This case was selected because that the fluid kinematics decay with decreasing water depth, and it is interesting to study the effects of the resolutions of wave points near the free surface. In the other cases the wave points were all evenly spaced.

As shown in the eigen value analysis, only in relatively short waves were the resonance motions excited, and in short waves the responses are more sensitive to the interpolation resolution due to the shorter wave lengths compared with long waves. Hence, the environmental conditions for the sensitivity study focused on relatively short waves with two wave directions, as shown in Table 5. Note that the ratio between the gap and the wave length can be used to characterise the convergence. Thus, the regular wave lengths λ with periods equal to the irregular wave peak periods were also included in Table 5 for reference.

Fig. 13 compares the extreme response statistics with different wave point resolutions in the XY plane and in the Z direction. The extreme values presented are the mean values of the maximum responses from 20 irregular wave seeds during the lowering phase. The results in the horizontal plane show that the results from the first three cases are close to each other with errors of the responses in case 2 and case 3 being less than 5% compared with case 1. However, the results from case 4, which had gaps of 8 metres, deviate from those with higher resolutions. For some responses, e.g., the monopile tip motions and rotations, the errors are approximately 10% to 20% compared with case 1. Therefore, a resolution with gaps of 4 metres in the XY plane was chosen in the time-domain simulations.

Similarly, the results in the vertical direction show increasing errors with decreasing resolutions, and

the errors of the motions and rotations of the monopile in case 8 are approximately 5% to 10% in most of the environmental conditions. The differences in the results from cases 6 and 7 are minor, which indicates that the responses were not very sensitive to resolution near the free surface. This is due to the extreme responses occurred at a large draft in which the wave forces on the monopile are the summation of the forces from all the strips instead of dominated by the forces at strips near the free surface. However, for structures with a smaller draft and large dimension in horizontal plane the extreme responses occur when the structures are near the free surface. The resolution of wave points near the free surface might be critical, and therefore higher resolutions should be used. In this study, a resolution of 2 metres in the vertical direction was used.

6 RESULTS AND DISCUSSION

6.1 Operational criteria

The operational criteria of the lifting operation of a monopile should be established by assessing the whole installation phase, including the upending, lowering and landing operations. Because this study is limited to the lowering phase, the critical responses of this phase are given.

1. Lift wire tension. The tension in the lift wire should never exceed the maximum working load of the wire, which depends on the property of the wire. According to DNV-RP-H103 [23], a slack wire and snap forces should be both avoided. In addition, extreme dynamic loads on the wire should be limited by checking the dynamic amplification factor (DAF) [23].

2. Gripper contact force. The gripper device was the main support structure that controlled the horizontal motions of the monopile. The relative motion between the monopile and the gripper induced huge impulse forces. The extreme contact loads should be estimated in order to perform the structural analysis of both the gripper device and the monopile to ensure their structural integrity at different environmental conditions.

3. Monopile motions. The motions of the monopile, particularly its rotations and the displacements of its end tip, affect the landing process that follows the lowering process examined in this study. Extreme motions should be estimated to ensure a successful landing at the designated position.

This study focuses on predicting the extreme responses during the lowering phase in various environmental conditions. Operational criteria should be established by further analysis, e.g., a structural analysis based

on the predicted extreme responses. By applying these criteria, safe operational environmental conditions could be predicted. The results of the time-domain simulations presented below will focus on the critical responses given above.

6.2 Response time series and spectra

Fig. 14 and Fig. 15 show the time history of the responses of the lifting system during lowering at two wave conditions. The responses in the figures include the motions of the monopile end tip, the contact forces of the gripper and the tensions in the lift wire. The lowering phase started when the winch was activated at 300 *sec*. The monopile was lowered though the splash zone until the winch stopped at 700 *sec*. During the process, the length of the lift wire increased with a fixed speed, and the added mass of the structure increased with its submergence. Both increases contributed to a continuous decrease in the natural frequencies of the lifting system. While the increasing wave forces acting on the monopile induced motions, the gripper device was placed to control its horizontal motions.

Comparing the responses in incident and disturbed waves shows that in short waves with $T_p = 5\ sec$ and $Dir = 45\ deg$, the rotations of the monopile, lift wire tensions and contact forces of the gripper device are significantly reduced when shielding effects are considered, whereas in long waves with $T_p = 11\ sec$ the influence of shielding effects is much less. These results again indicate that the shielding effects of the vessel have more influence on the fluid kinematics in short waves, which is consistent with the RAOs of the fluid kinematics shown in Fig. 8.

The response spectra of the lowering phase were obtained using Fourier transformation of the time series. Fig. 16 shows the response spectra at $T_p = 5\ sec$ and 11 *sec* with direction $Dir = 45\ deg$. In short waves, the resonant motions of the monopile are excited near the wave period, which corresponds to the peak frequency of the spectrum. The hydrodynamic wave loads on the monopile dominate the response of the system in this case. In long waves, however, there are two peaks in the motion spectrum. The frequencies of the secondary peak with $\omega \approx 1.1\ rad/s$ match the natural frequencies of the monopile rotational motion, while the frequencies of the main peak with $\omega \approx 0.5\ rad/s$ are the wave spectrum peak frequencies. Due to the couplings of the monopile and the vessel, the increasing response of the vessel in long waves dominates the motions of the monopile. The peak frequency of the wire tension is consistently twice of the rotational peak frequency, which means that one cycle of rotational motion induces two cycles of variations in the wire tension.

For both wave conditions, the peaks at $\omega \approx 1.1\ rad/s$ in the response spectra, which is close to

the natural frequency of the rotational motions of the monopile, are significantly reduced when the shielding effects of the vessel are considered. However, in long waves with $T_p = 11$ sec the response peaks corresponding to the long wave peak period do not decrease in disturbed waves. These results indicate the significant influence of the shielding effects on the monopile motions, particularly in short waves when the wave frequencies are close to the natural frequencies of the monopile.

6.3 Response statistics

Fig. 17 compares the extreme values of the critical responses during the lowering process in incident and disturbed waves with a wave direction of 45 deg. These extreme values presented are the mean values of the maximum responses from 20 irregular wave seeds used in the lowering phase. The extreme monopile tip distance in the figures refers to the maximum offset of the monopile tip from the designated landing position in the XY plane during lowering. The rotational motions of the monopile in the figure are the maximum rotations relative to the horizontal plane and were calculated by combining the pith and roll motions. The responses of the lifting system were sensitive to the shielding effects of the vessel as shown.

In incident waves, the extreme responses of the lifting system first decrease and then increase as the wave length increases. The maximum rotations and tip distances occur at $T_p = 6$ sec, which is close to the natural periods of the rotations. The rapid increase in the motions and rotations in long waves is due to the increasing crane tip motions that are induced by the vessel motion (see Eqn. 6). The extreme motions of the crane tip in X and Y directions at varying wave periods are shown in Fig. 18. The main contribution to the rapid increase in the crane tip motions comes from the vessel roll motion at a large lifting height. It should be mentioned that the increasing distance from the monopile tip to the designated position would result in difficulty during the landing operations and huge landing forces if the landing devices were used at the designated position as discussed in [21]. Fig. 18 also indicates that the effects of the monopile motions on the vessel motions are negligible. Because the gripper contact forces and lift wire tensions are more dependent on monopile motions at its own natural periods, these extreme responses do not increase as much as the monopile motions in long waves as shown in Fig. 17.

In the disturbed wave filed, the extreme responses are greatly reduced in short waves compared with long waves with $Dir = 45$ deg. As shown above, the fluid kinematics in disturbed wave field depend greatly on the wave directions; the shielding effects of the vessel on the responses of the lifting system are expected to vary with wave direction. The comparison of the RAOs at $Dir = 0$ deg and $Dir = 45$ deg in Fig. 8 suggests that at smaller wave directions the shielding effects would be reduced, particularly

in short waves. Therefore, the current results at Dir =45 deg do not represent the shielding effects at different wave directions. Results at various wave directions are required.

6.4 Responses at different wave directions

The sensitivity of the extreme responses at different wave directions was studied. Figs. 19 compares the statistics of the extreme rotations of the monopile in disturbed waves with those in incident waves at four irregular wave conditions.

In incident waves, the responses with waves coming from the port side are similar to the responses with waves coming from the starboard side due to the symmetry of the vessel about its X axis. This means the responses are independent of whether the monopile is in the windward side (Dir = 180 to 360 deg) or the leeward side (Dir = 0 to 180 deg) of the vessel. However, when shielding effects are taken into account, the responses are greatly affected.

In relatively short waves (T_p = 5 and 7 sec), the responses are significantly reduced when the monopile is placed on the leeward side of the vessel when shielding effects are considered, and the rotational motions of the monopile and wire tension greatly increase when the monopile is on the windward side of the vessel. Therefore, the lifting operation should be performed on the leeward side of the vessel to utilise the shielding effects of the vessel. With increasing wave length, the differences between the extreme responses in disturbed and incident waves are rapidly reduced. The directional plots show that the responses in both incident and disturbed waves are almost symmetric about the beam sea direction because the installation of the monopile was carried out close to mid-ship in the longitudinal direction.

When only the extreme responses of monopile rotations from Dir = 0 to 90 deg are considered, the extreme responses reach their minimum values at approximately Dir = 45 to 60 deg in short waves, whereas in long waves the minimum values occur at approximately Dir = 15 to 30 deg. Both the resonance motions of the monopile and the vessel motions affect the responses of the lifting system, and the factor that dominates the responses depends on both the wave direction and the wave length.

As shown in the eigen value analysis, in short waves, the resonance motions of the monopile were excited and affected the responses of the lifting system. The RAOs of the fluid kinematics near the monopile position varied with the wave direction and in general reached a minimum near the beam sea condition (Dir = 90 deg), and they increased gradually when the direction moved towards following sea or heading sea conditions. Hence, the resonance motions of the monopile decreased from Dir = 0 deg to 90 deg. On the other hand, although the vessel motions were minor in short waves, the crane tip

motions always increased as the wave direction moves from heading sea to beam sea conditions due to the roll motion of the vessel and the large lift height. Thus, near heading sea conditions, the resonance motion dominated and the extreme responses decreased as the wave direction moved to quartering sea conditions. However, when the direction increased further, due to the increase in the vessel roll motion and the decrease in the resonance motion, the crane tip motions began to dominate the response of the system. Hence, the extreme responses increased again until $Dir = 90\ deg$. The minimum values were approximately $Dir = 45$ to $60\ deg$.

However, in long waves, the resonance motion of the monopile was secondary because the wave peak periods were away from the eigen periods of the monopile. At the same time the vessel motions increased significantly so that the crane tip motions dominated the responses of the system even at a relatively small wave direction of approximately 15 to 30 deg. Thus, the responses continued to increase when the wave direction increased towards beam sea conditions.

Therefore, the minimum extreme responses at different sea states occurred at different wave directions. In order to utilise the shielding effects to increase the weather window as much as possible, the most suitable wave directions at different wave lengths should be applied.

Because the motions of the monopile are dominated by the vessel motion in long waves, the lift wire and the gripper control the motions of the monopile in a way that follows the motions of the vessel. At $T_p = 11\ sec$, the rotational motions of the monopile decreased slightly at $Dir = 0$ to $180\ deg$; thus, the extreme tensions in the lift wire in disturbed waves were very close to those in incident waves in all wave directions. In spite of this, the extreme gripper contact forces were greatly decreased at $Dir = 0$ to 180 deg. This is due to the high stiffness of the gripper device and the sensitivity of the contact force to the monopile rotational motions. Therefore, to reduce the contact forces, the lifting operation should be conducted in the leeward side of the vessel even in very long waves.

The differences in the extreme responses in disturbed and incident waves, including the extreme rotations of the monopile, the extreme tensions in the lift wire and the extreme contact forces of the gripper are quantified in Table 6 at directions from 0 deg to 90 deg at four wave period conditions. The ratios in the table are given as percentages and were calculated as the difference of the responses in disturbed and incident waves divided by the response in incident waves. The bold figures show the maximum reduction of the responses in different wave periods. The corresponding wave directions are shown to decrease with increasing wave period.

The maximum decrease in the responses in short waves is approximately 70% for both monopile

rotational motion and gripper contact force. In long waves ($T_p = 11\ sec$), the ratios become approximately 35% and 50%, respectively, which shows the decrease in shielding effects with increasing wave period. The reduction in the tensions in the lift wire is somewhat less compared with the other two responses.

6.5 Comparison of responses using floating and jack-up vessels

The jack-up installation vessel is another choice in the installation of a monopile. The hull of the jack-up vessel is raised above the sea surface on legs, and the vessel is fixed to the sea bed during lifting operations. The greatest advantage of a jack-up vessel is that it provides a stable working platform for lifting operations so that only the wave forces on the monopile itself matter during the lowering phase. However, because only the legs of the jack-up vessel are in the water during the operation, the shielding effects from the jack-up vessel are very small and can be ignored. Thus, the waves on the monopile are incident waves in all wave directions, and may induce larger motions compared with the disturbed waves that occur when the floating vessel is used. It is interesting to compare the responses of these two types of vessel to select the most suitable vessel in different environmental conditions.

Fig. 20 compares the extreme monopile rotations in different wave directions when using the jack-up vessel and the floating vessel. The responses when using the floating vessel were calculated to include the shielding effects of the vessel, whereas only the incident waves were considered in the case of the jack-up vessel.

In short to intermediate waves, the resonance motions of the monopile dominated; thus, the extreme rotations when using the floating vessel were lower than using jack-up vessel at $Dir = 0$ to 180 deg due to the shielding effects of the floating vessel. With increasing wave length, the motions of the floating vessel increased and began to dominate the responses, and hence the responses when using the floating vessel exceeded those when using the jack-up vessel, particularly in large wave directions. The responses were even larger when using the floating vessel if the installation was performed in the windward side of the vessel.

Therefore, to reduce the extreme responses, it is better to use the floating vessel in short to intermediate waves and to use the shielding effects of the vessel, whereas in long waves (in the current model $T_p > 11$ sec), the jack-up vessel is better. If the floating vessel is used in long waves, the operations should be carried out close to heading seas or following seas to avoid large roll motions of the vessel.

7 CONCLUSIONS

In this study, a numerical coupled model of lowering an offshore wind turbine monopile was established. A continuous lowering process was analysed. The effects of vessel shielding on the responses of the lifting system were calculated by establishing an external DLL and implementing it in SIMO. The wave forces on the monopile were calculated during lowering by interpolating fluid kinematics between pre-defined wave points near the floating vessel. It is concluded that the shielding effects from the vessel reduce the extreme responses of lifting operations conducted in the vicinity of the vessel at proper vessel heading angles. The shielding is more significant in short waves than in long waves.

The fluid kinematics in disturbed waves show a great dependence on the wave direction; the RAOs are reduced when the wave comes from the leeward side of the vessel and may increase greatly when the wave comes from the windward side. In addition, the shielding effects of the vessel depend greatly on the position of the lifted object relative to the vessel. The reduction in the extreme responses that results from shielding effects is expected to decrease when the lifted object is located further away from the vessel.

The numerical simulations show that the extreme responses, i.e., the rotations of the monopile, the tension in the lift wire and the contact force of the gripper, reached minimum values at wave directions of approximately $Dir = 45$ to 60 deg in short waves, and the extreme motions of the monopile in disturbed waves could be reduced by more than 50% compared with those in incident waves. In long waves, the minimum extreme values were acquired at directions approximately $Dir = 15$ to 30 deg, and the reduction of the extreme rotation and gripper contact force is greater than 30% due to shielding effects. Therefore, the responses can be greatly overestimated in the design of marine operations if shielding effects are not considered. This fact implies an underestimation of the weather window in such operations.

Although the shielding effects of the vessel cause a great reduction in the extreme responses at many sea conditions, the vessel heading angle should be adjusted carefully in very long waves that have peak periods close to the natural periods of the vessel, conditions in which the vessel motions can induce severe motions in the lifted object through the crane tip. Use of a jack-up vessel is recommended in cases of very long waves to prevent these large crane tip motions that are induced by floating vessels.

The approach proposed in this study to consider the shielding effects of the vessel is also applicable to simulating operations of more complicated structures, such as jacket foundations and sub-sea templates, which can be modelled as a collection of separate slender elements [24]. For continuous lowering simulations

of large volume structures such as gravity-based structures (GBS), the hydrodynamic coupling between the vessel and the GBS must be calculated continuously with an increasing draft of the GBS using numerical method such as panel method to consider the shielding effects of the vessel, which is beyond the capability of the current approach. Another limitation of the current approach is that only long-crested waves are considered. The vessel crane tip motions as well as the shielding effects from the vessel will be influenced by the spreading of the waves. The shielding effects are expected to be less in short-crested waves than in long-crested waves, especially in short waves with vessel heading close to beam seas. Moreover, the most suitable directions that have the minimum extreme responses might also shift if short-crested waves are considered. The influence of the short-crested waves on the shielding effects will be studied in the future.

Acknowledgments

The authors gratefully acknowledge the financial support from the Research Council of Norway granted through the Department of Marine Technology, Centre for Ships and Ocean Structures (CeSOS) and Centre for Autonomous Marine Operations and Systems (AMOS), NTNU. Thanks are extended to Wilson Guachamin Acero and Erin Bachynski from CeSOS for valuable discussions.

References

[1] K. Thomsen, *Offshore wind: A comprehensive guide to successful offshore wind farm installation.* Academic Press, 2011.

[2] A. Moller, "Efficient offshore wind turbine foundations," in *POWER EXPO 2008 - International Exhibition on Efficient and Sustainable Energy*, 2008.

[3] K. Aarset, A. Sarkar, and D. Karunakaran, "Lessons learnt from lifting operations and towing of heavy structures in north sea," in *Offshore Technology Conference, May 2-5, Houston, Texas, USA*, 2011.

[4] R. Gordon, G. Grytoyr, and M. Dhaigude, "Modelling suction pile lowering through the splash zone," in *Proceedings of the 32nd International Conference on Ocean, Offshore and Arctic Engineering, June 9-14, Nantes, France*, 2013.

[5] M. Graczyk and P. Sandvik, "Study of landing and lift-off operation for wind turbine components on a ship deck," in *Proceedings of the 31st International Conference on Ocean, Offshore and Arctic Engineering, July 1-6, Rio de Janeiro, Brazil*, 2012.

[6] M. Perry and P. Sandvik, "Identification of hydrodynamic coefficients for foundation piles," in *Proceedings of the 15th international Offshore and Polar Engineering Conference, June 19-24, Seoul, Korea*, 2005.

[7] van der Wal R., H. Cozijn, and C. Dunlop, "Model tests and computer simulations for njord fpu gas module installation," in *Marine Operations Specialty Symposium, Singapore*, Research Publishing Services, 2008.

[8] P. Sandvik, "Estimation of extreme response from operations involving transients," in *Proceedings of the 2nd Marine Operations Specialty Symposium, Singapore*, 2012.

[9] P. Mukerji, "Hydrodynamic responses of derrick vessels in waves during heavy lift operation," in *20th Offshore Technology Conference, Houston*, 1988.

[10] H. van den Boom, J. Dekker, and R. Dallinga, "Computer analysis of heavy lift operations," in *22nd Offshore Technology Conference, Houston*, 1990.

[11] J. Baar, J. Pijfers, and J. Santen, "Hydromechanically coupled motions of a crane vessel and a transport barge," in *24th Offshore Technology Conference, Houston*, 1992.

[12] DNV, *Recommended Practice DNV-RP-C205, Environmental Conditions and Enviromental Loads*, October 2010.

[13] MARINTEK, *SIMO - Theory Manual Version 4.0*, 2012.

[14] K. Park, J. Cha, and K. Lee, "Dynamic factor analysis considering elastic boom effects in heavy lifting operations," *Ocean Engineering*, vol. 38, no. 10, pp. 1100–1113, 2011.

[15] DNV, *Wadam theory manual.* Det Norske Veritas, 2008.

[16] O. Faltinsen, *Sea Loads on Ships and Ocean Structures.* Cambridge University Press, 1990.

[17] S. Mavrakos, "Wave loads on a stationary floating bottomless cylindrical body with finite wall thickness," *Applied Ocean Research*, vol. 7, no. 4, pp. 213–224, 1985.

[18] S. Mavrakos, "Hydrodynamic coefficients for a thick-walled bottomless cylindrical body floating in water of finite depth," *Ocean Engineering*, vol. 15, no. 3, pp. 213–229, 1988.

[19] C. Garrett, "Bottomless harbours," *Journal of Fluid Mechanics*, vol. 43, no. 03, pp. 433–449, 1970.

[20] X. Zheng, "Random wave forces on monopile wind turbine foundations: a comparison of wave models," in *Proceedings of the 32nd International Conference on Ocean, Offshore and Arctic Engineering, June 9-14, Nantes, France*, 2013.

[21] L. Li, Z. Gao, and T. Moan, "Numerical simulations for installation of offshore wind turbine monopiles using floating vessels," in *Proceedings of the 32nd International Conference on Ocean, Offshore and Arctic Engineering, June 9-14, Nantes, France*, 2013.

[22] C. Lee, *WAMIT theory manual.* Massachusetts Institute of Technology, Department of Ocean Engineering, 1995.

[23] DNV, *Recommended Practice DNV-RP-H103, Modelling and Analysis of Marine Operations*, April 2011.

[24] T. Jacobsen and B. Leira, "Numerical and experimental studies of submerged towing of a subsea template," *Ocean Engineering*, vol. 42, pp. 147–154, 2012.

List of Figures

1 Monopile lifting arrangement (a) and definitions of global coordinate system (b) 29

2 Non-dimensional $2D$ added mass coefficient 30

3 Illustration of (a) physical and (b) numerical models for gripper device coupling 30

4 Illustration of eigenmodes of monopile rigid body motions (eigenvectors are magnified by a factor of 10) 31

5 Eigen frequency of monopile rigid body motion vs. position and representative wave spectra 32

6 Interpolation of fluid kinematics in disturbed waves 32

7 Time-domain simulation approach considering vessel shielding effects 33

8 RAOs of fluid kinematics vs. wave frequency (x =-20 m, y = 30 m, z = 0 m) 34

9 RAOs of wave elevation and fluid particle velocities at varying directions (x =-20 m, y = 30 m, z = 0 m) 35

10 RAOs of wave elevation and fluid particle velocities vs. water depth (x = -20 m, y = 30 m) 36

11 RAOs of wave elevation of disturbed waves in XY plane (z = 0 m) 37

12 Parameters in sensitivity study of wave point resolution 37

13 Extreme response statistics with different resolutions in XY plane (a) and in Z direction (b). 38

14 Time series of responses in incident and disturbed waves (H_s = 2.5 m, T_p = 5 sec, Dir = 45 deg) 39

15 Time series of responses in incident and disturbed waves (H_s = 2.5 m, T_p = 11 sec, Dir = 45 deg) 40

16 Spectrum density of responses during lowering in incident and disturbed waves (H_s = 2.5 m) 41

17 Extreme responses of lifting system in incident and disturbed waves (H_s = 2.5 m, Dir = 45 deg) 42

18 Extreme crane tip motions in incident and disturbed waves (H_s = 2.5 m, Dir = 45 deg) . 43

19 Extreme rotations of monopile in incident and disturbed waves at different wave directions (H_s = 2.5 m) 44

20 Extreme monopile rotations by using jack-up and floating installation vessels at different wave directions (H_s = 2.5 m) 45

List of Tables

1 Main parameters of the floating installation vessel and the monopile 46

2 Main parameters of the mechanical couplings 46

3 Eigenperiods and eigenvectors of vessel rigid body motions 46

4 Eigenperiods and eigenvectors of monopile rigid body motions 47

5 Parameters for sensitivity study of wave point resolutions and environmental conditions . 47

6 Differences in percentage between extreme responses in disturbed and incident waves . . . 47

8 FIGURES

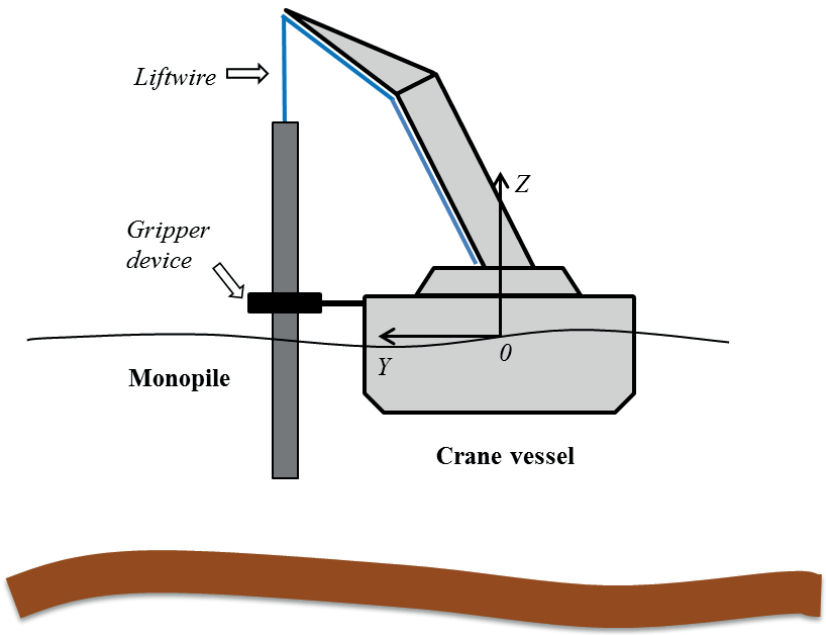

(a)

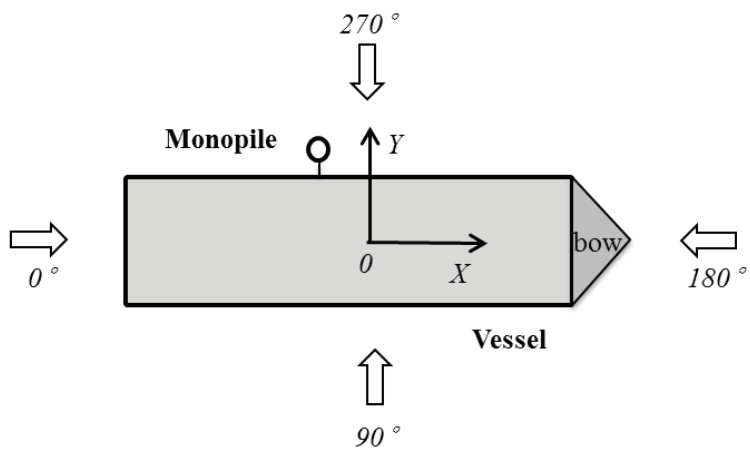

(b)

Fig. 1. Monopile lifting arrangement (a) and definitions of global coordinate system (b)

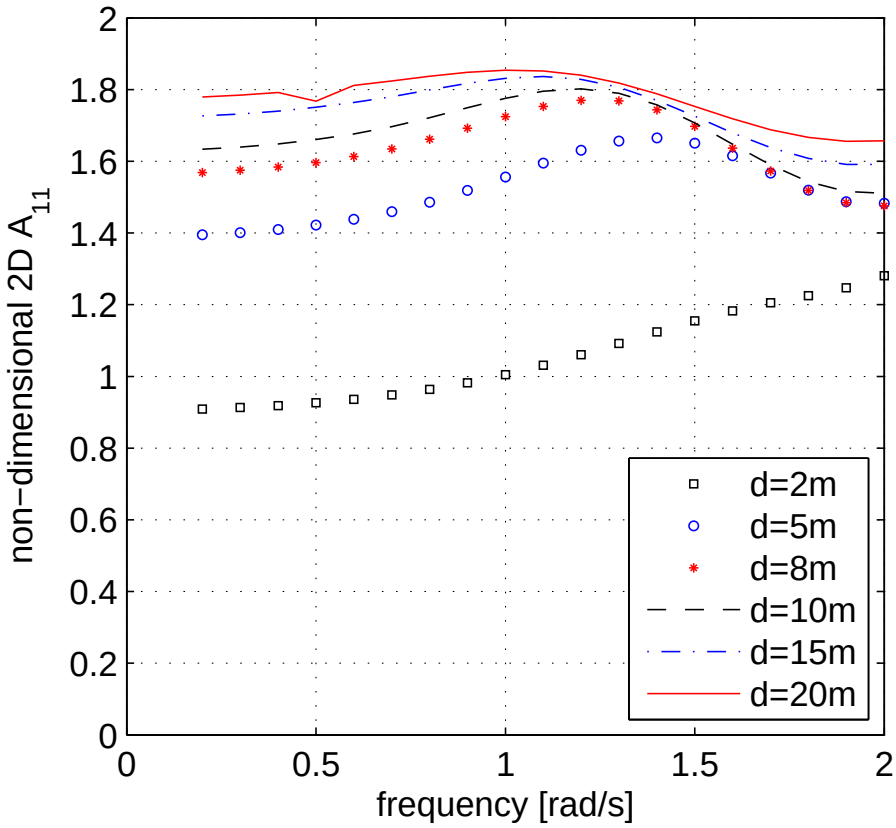

Fig. 2. Non-dimensional $2D$ added mass coefficient

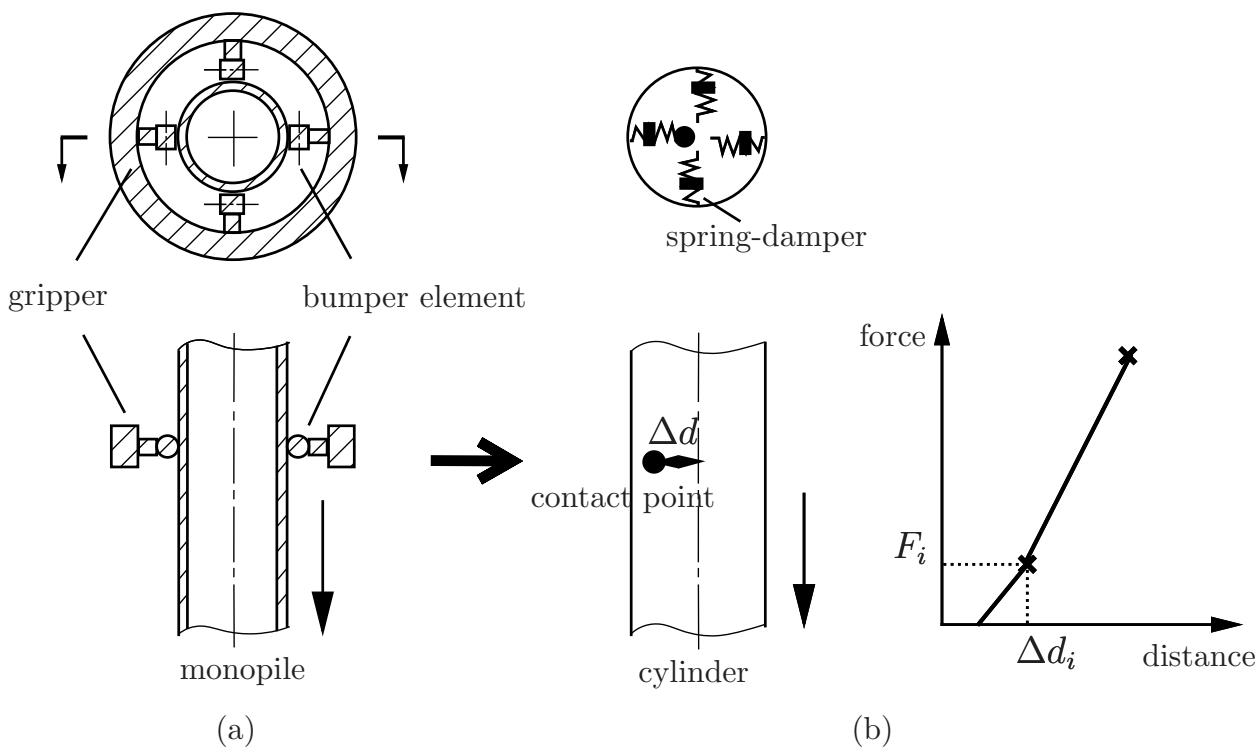

Fig. 3. Illustration of (a) physical and (b) numerical models for gripper device coupling

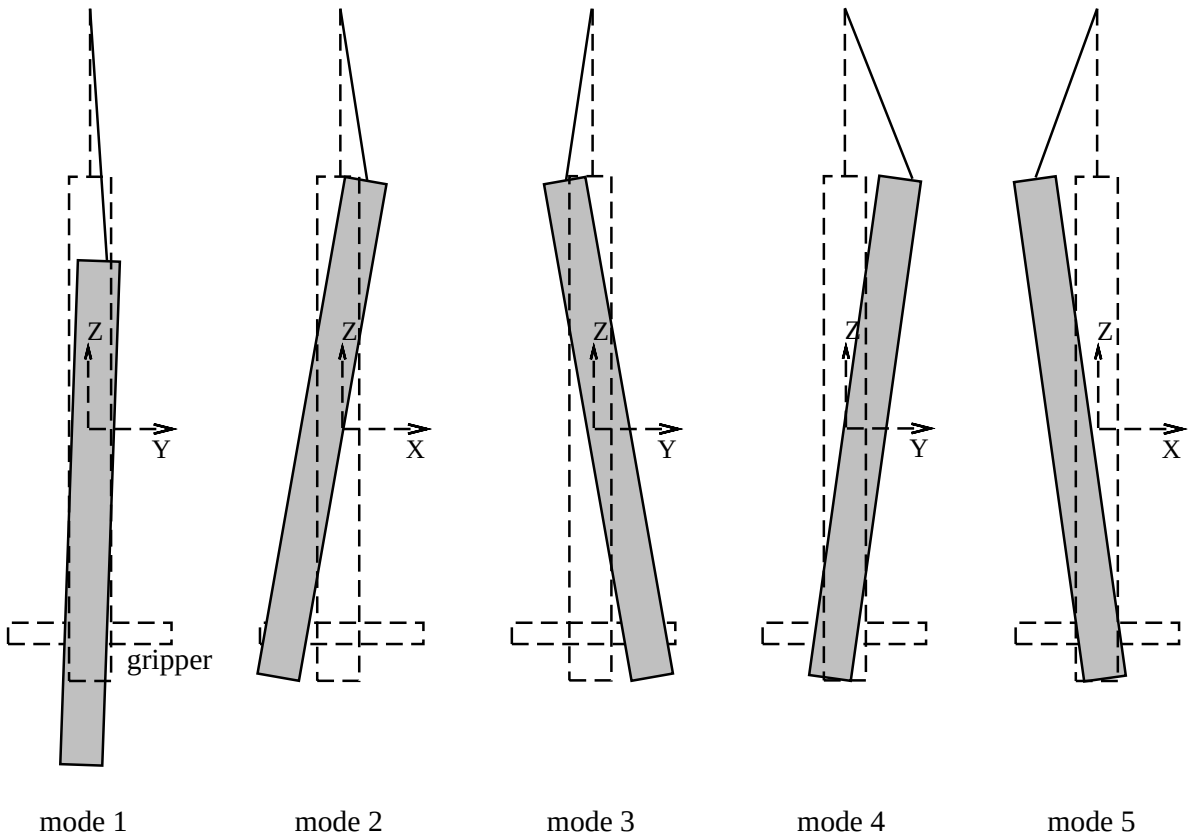

Fig. 4. Illustration of eigenmodes of monopile rigid body motions (eigenvectors are magnified by a factor of 10)

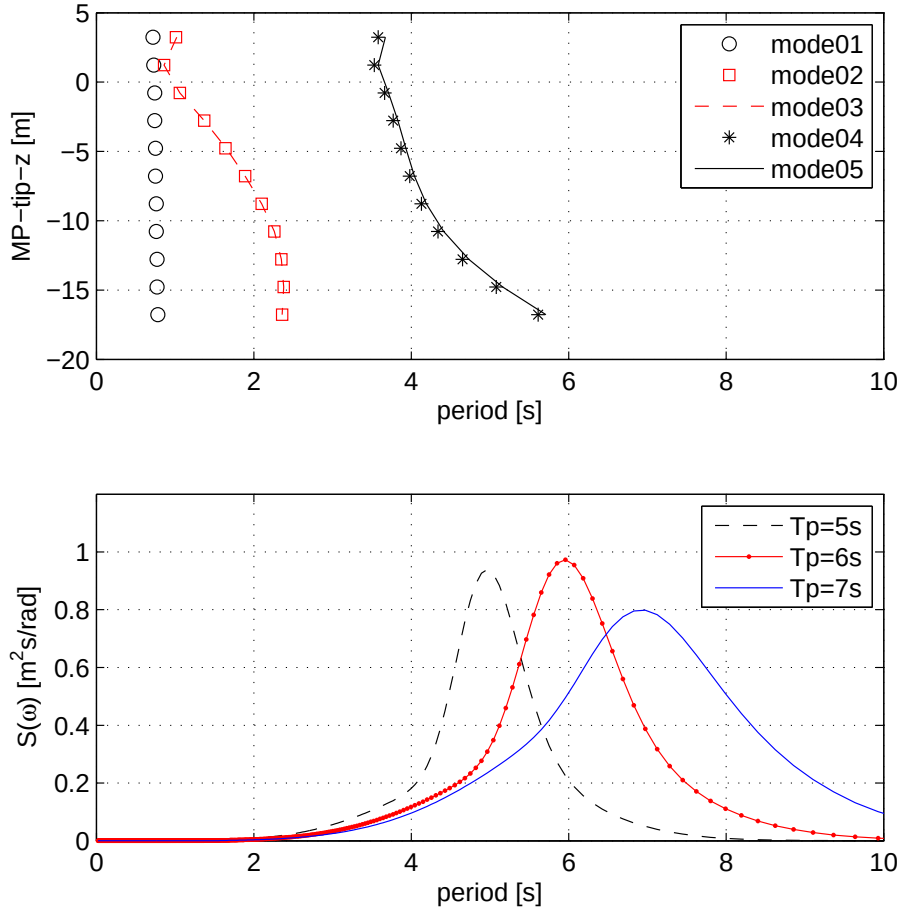

Fig. 5. Eigen frequency of monopile rigid body motion vs. position and representative wave spectra

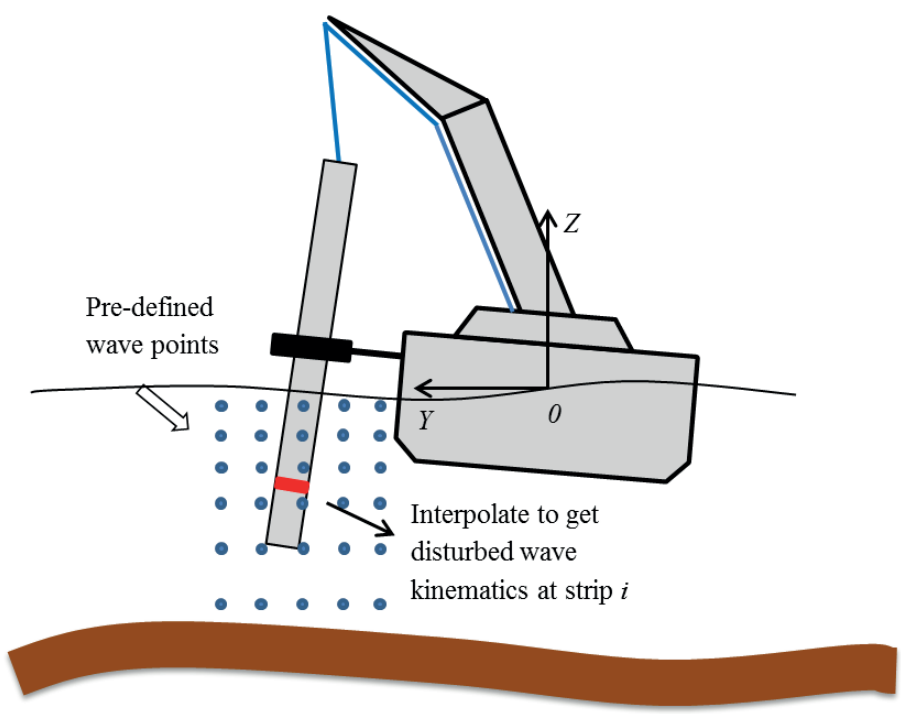

Fig. 6. Interpolation of fluid kinematics in disturbed waves

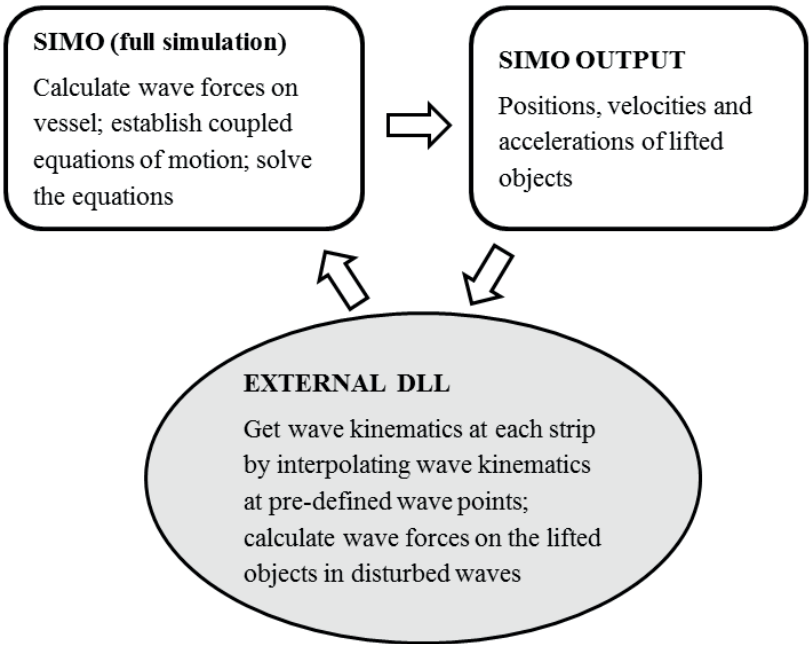

Fig. 7. Time-domain simulation approach considering vessel shielding effects

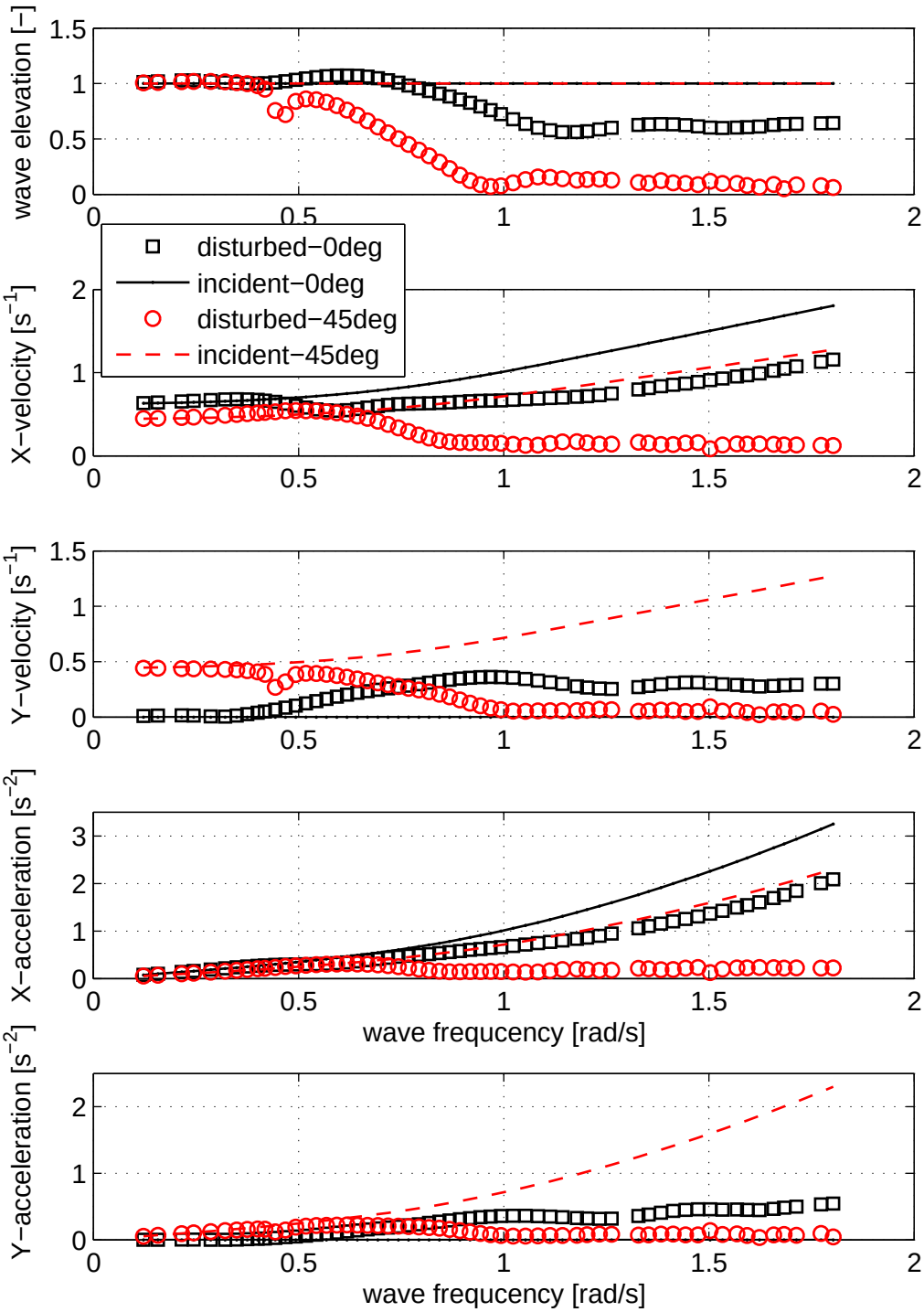

Fig. 8. RAOs of fluid kinematics vs. wave frequency (x =-20 m, y = 30 m, z = 0 m)

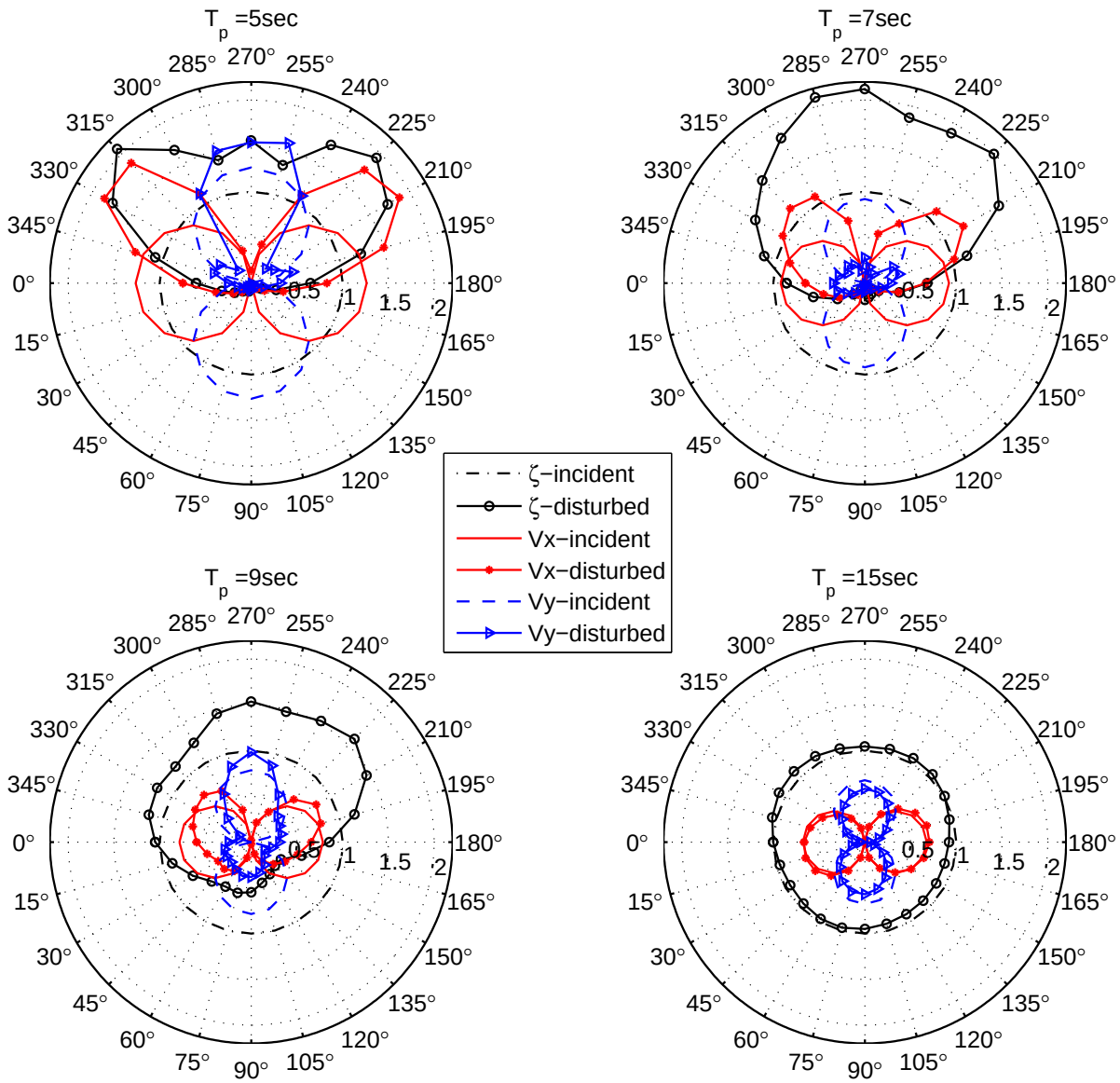

Fig. 9. RAOs of wave elevation and fluid particle velocities at varying directions (x =-20 m, $y = 30$ m, $z = 0$ m)

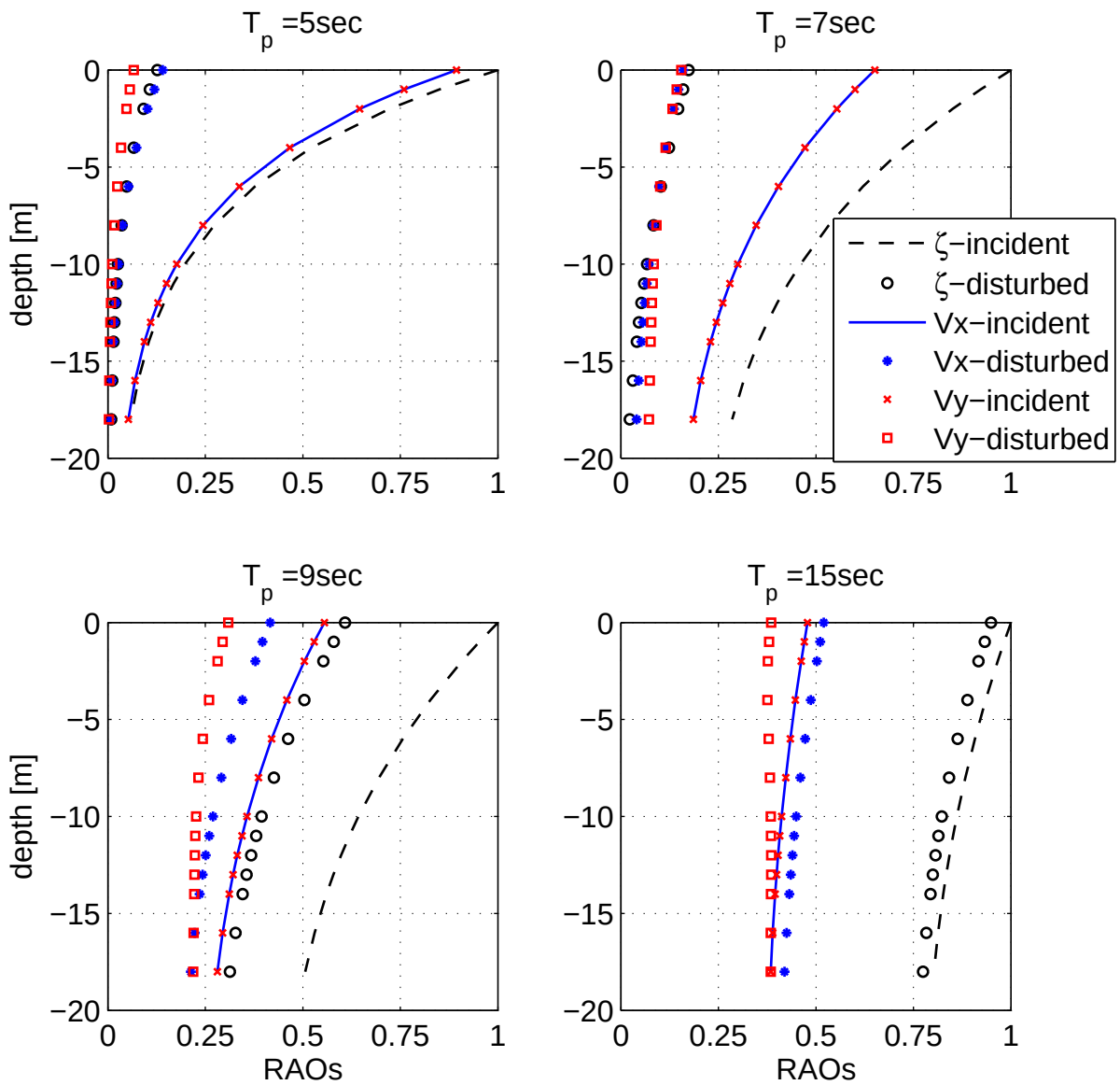

Fig. 10. RAOs of wave elevation and fluid particle velocities vs. water depth (x = -20 m, y = 30 m)

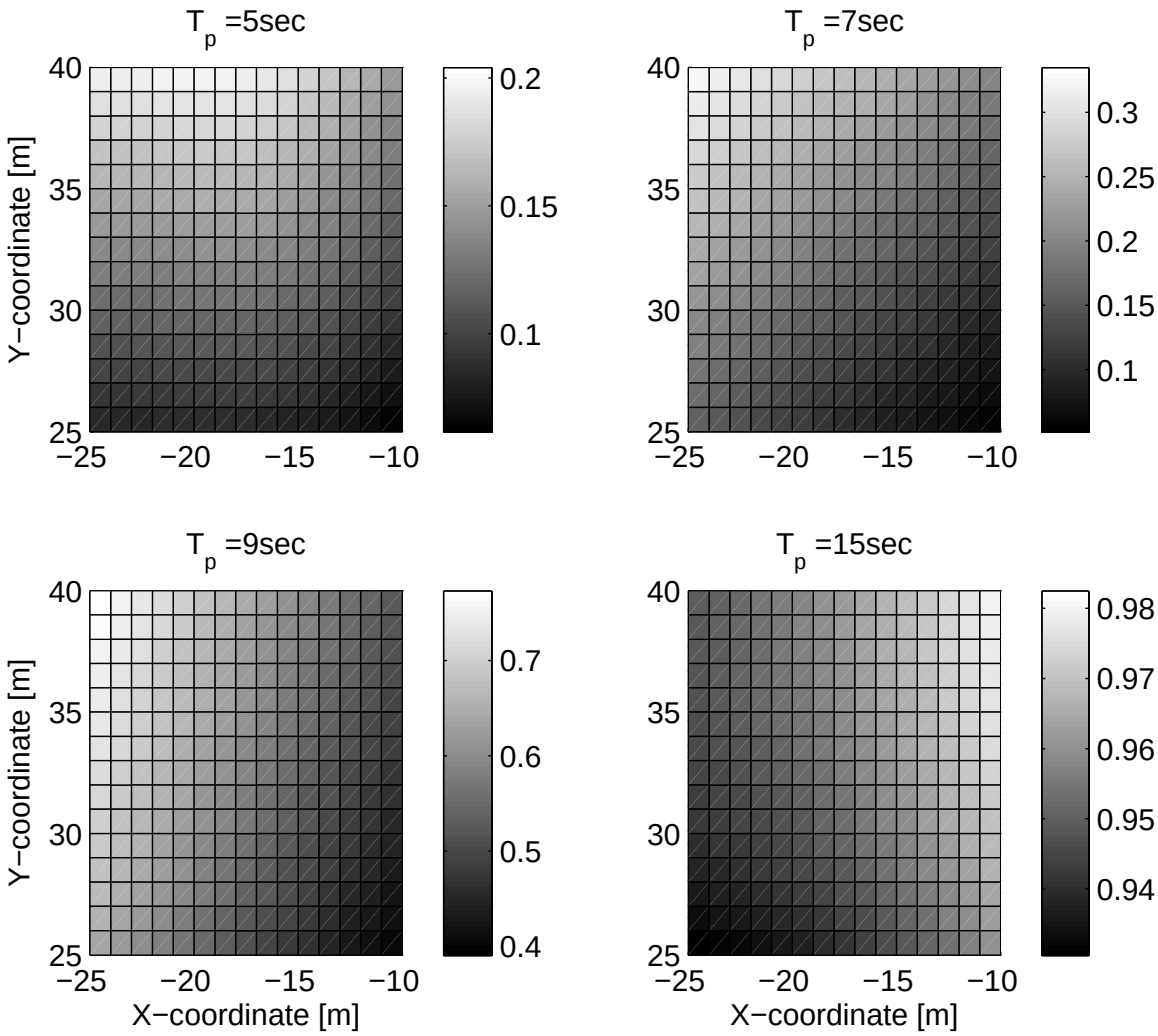

Fig. 11. RAOs of wave elevation of disturbed waves in XY plane ($z = 0\ m$)

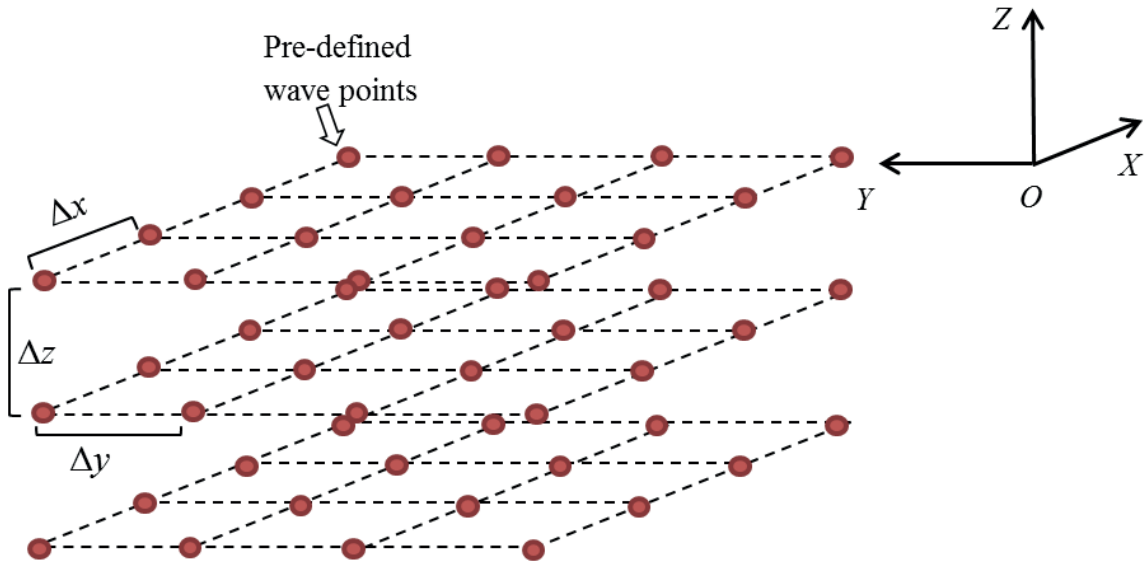

Fig. 12. Parameters in sensitivity study of wave point resolution

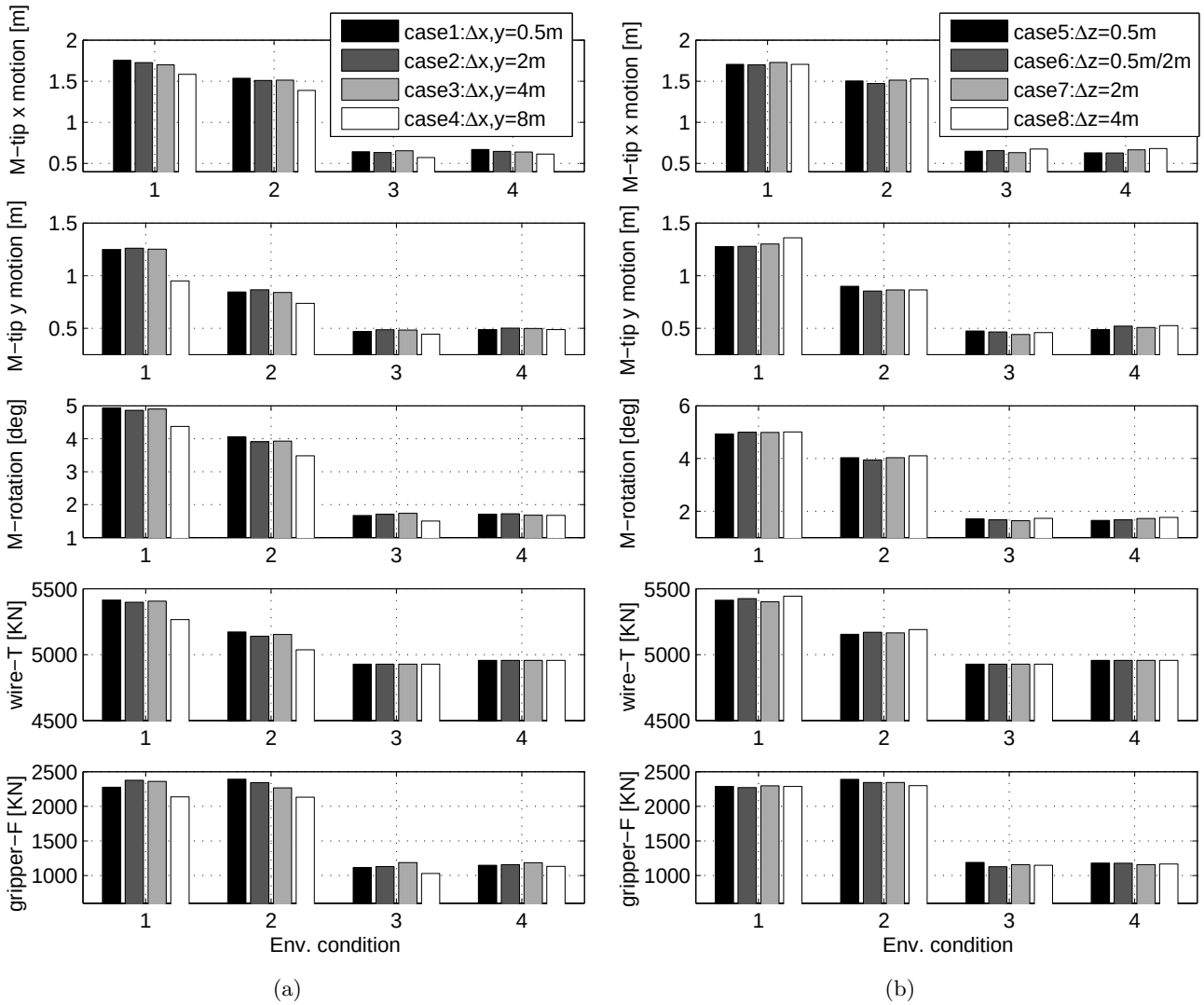

Fig. 13. Extreme response statistics with different resolutions in XY plane (a) and in Z direction (b).

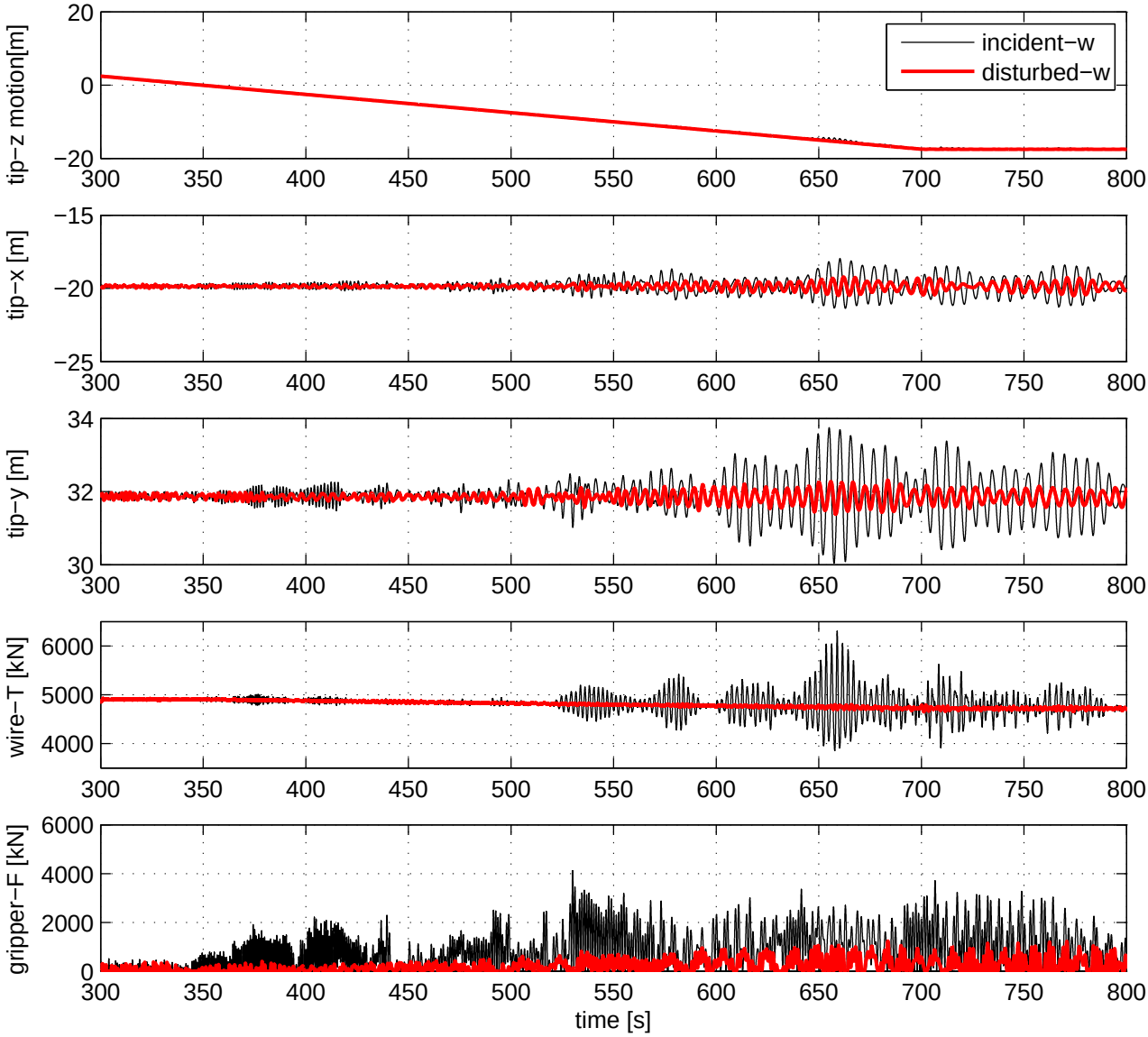

Fig. 14. Time series of responses in incident and disturbed waves ($H_s = 2.5\ m$, $T_p = 5\ sec$, $Dir = 45\ deg$)

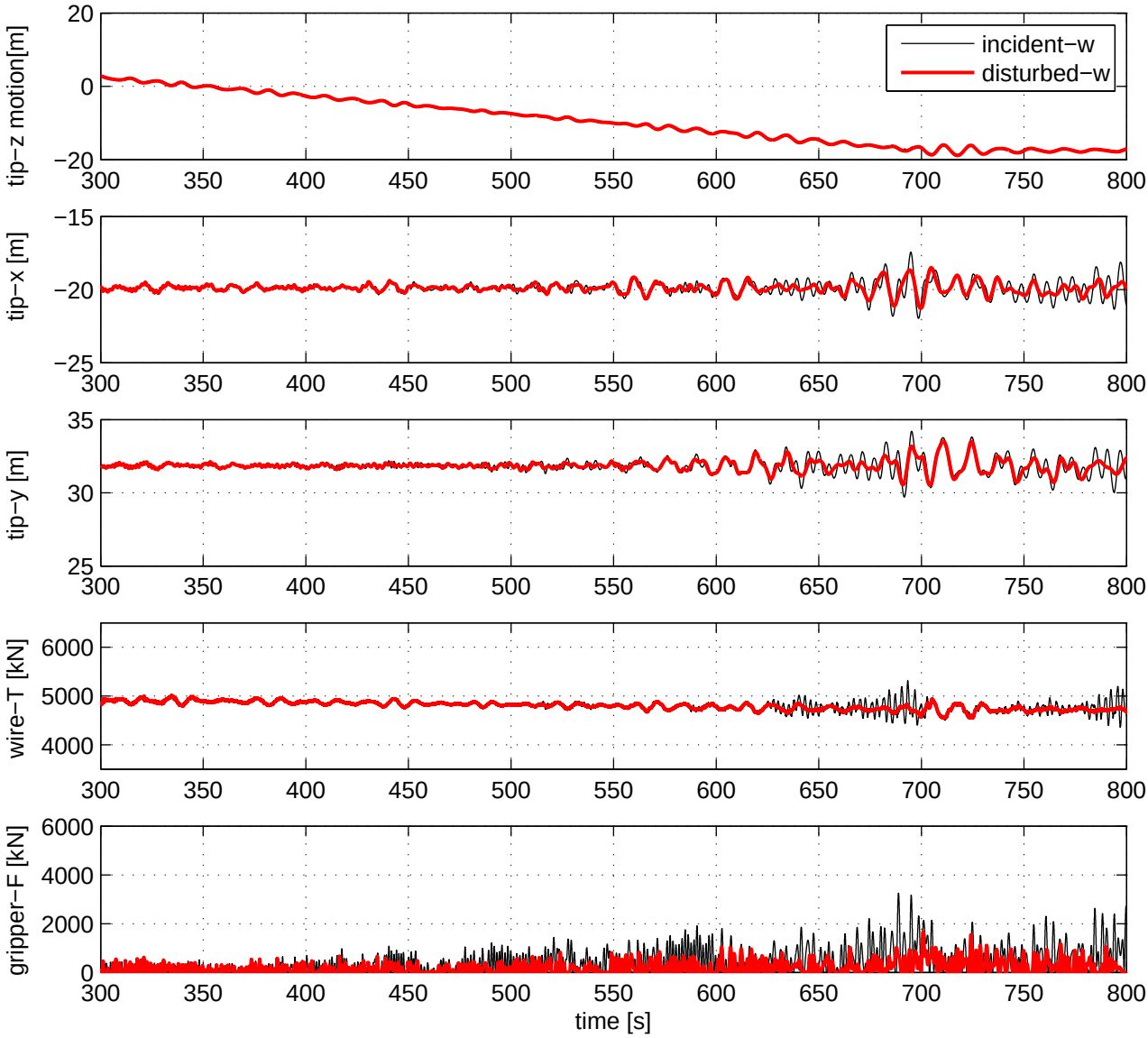

Fig. 15. Time series of responses in incident and disturbed waves ($H_s = 2.5\ m$, $T_p = 11\ sec$, $Dir = 45\ deg$)

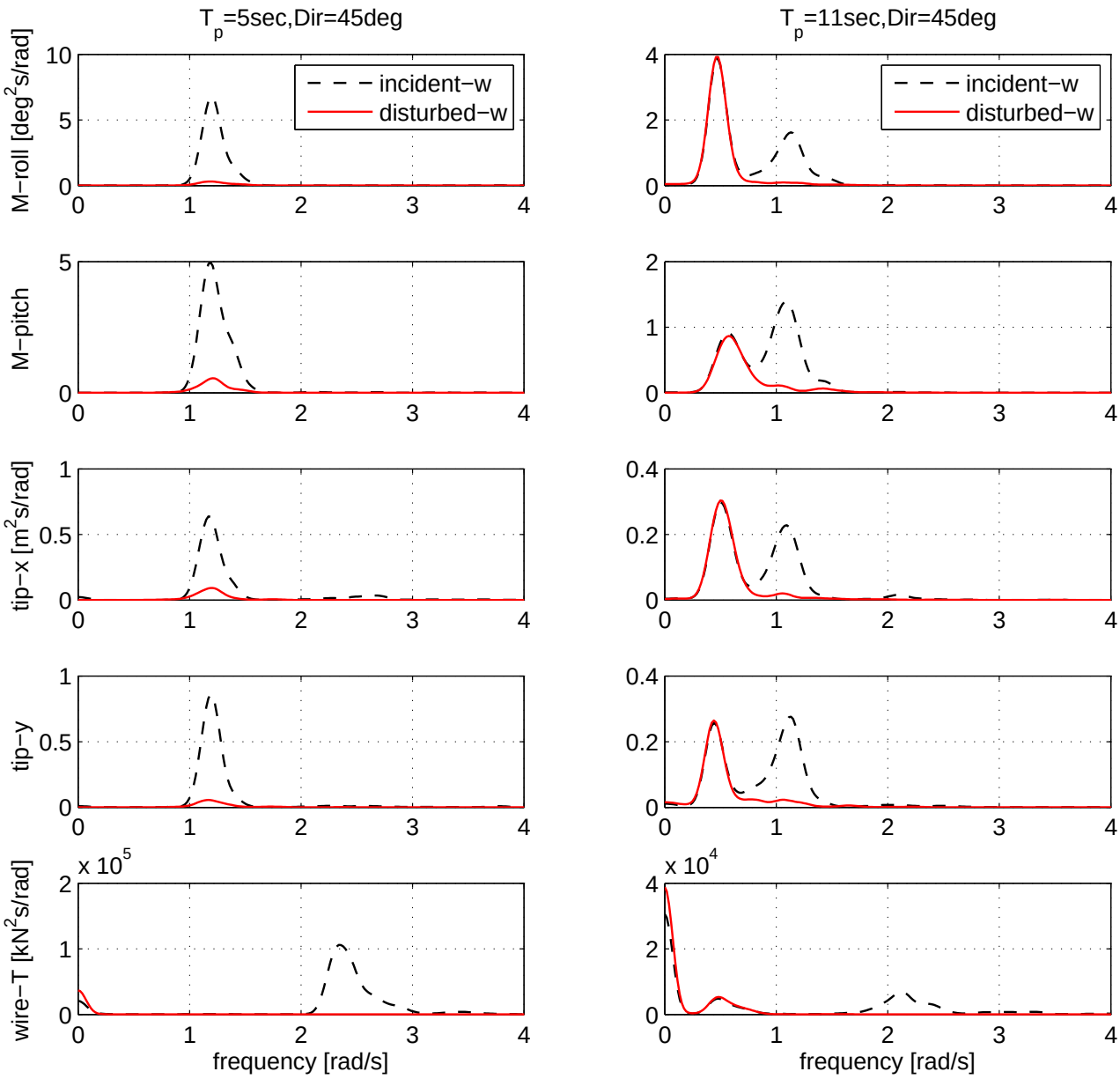

Fig. 16. Spectrum density of responses during lowering in incident and disturbed waves ($H_s = 2.5\ m$)

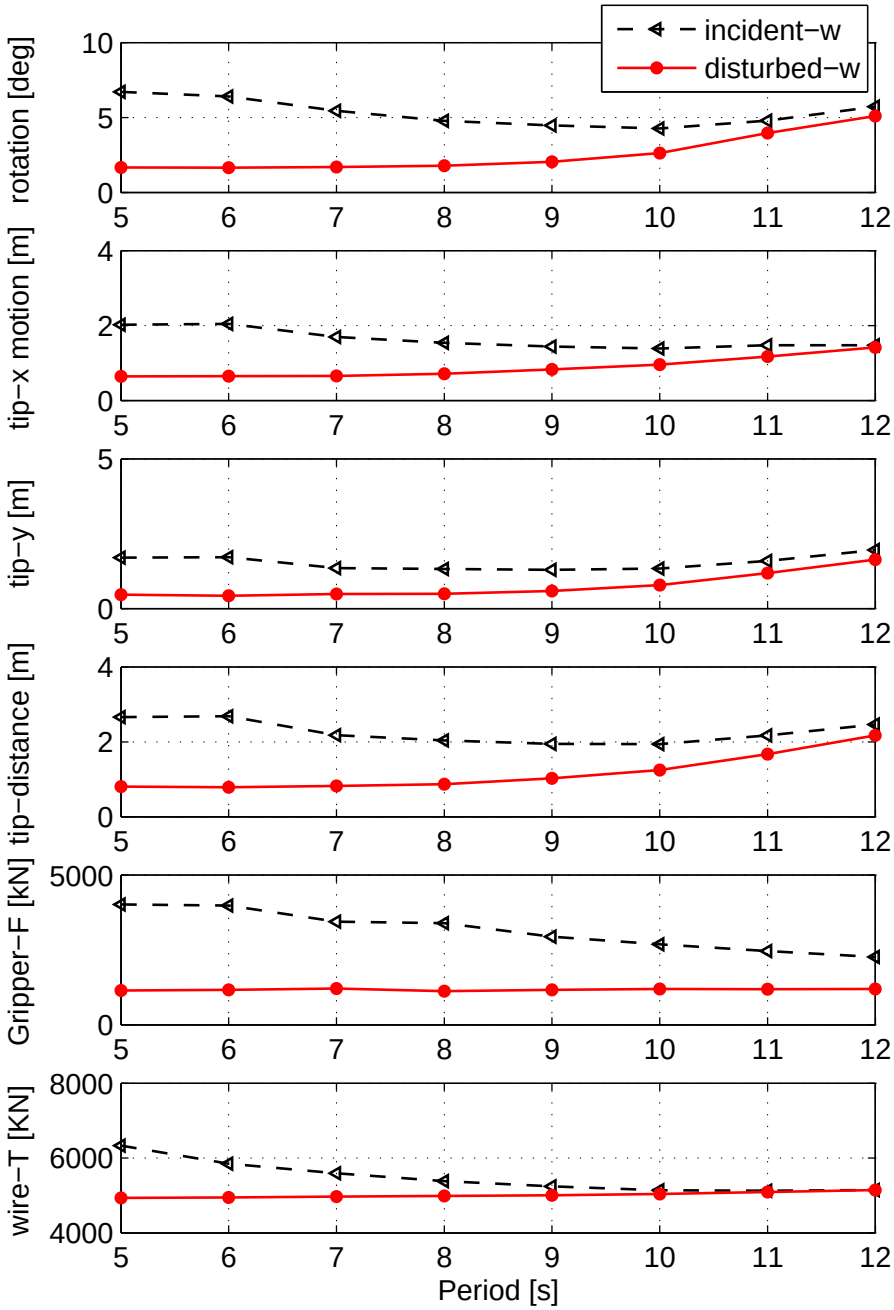

Fig. 17. Extreme responses of lifting system in incident and disturbed waves ($H_s = 2.5\ m$, $Dir = 45\ deg$)

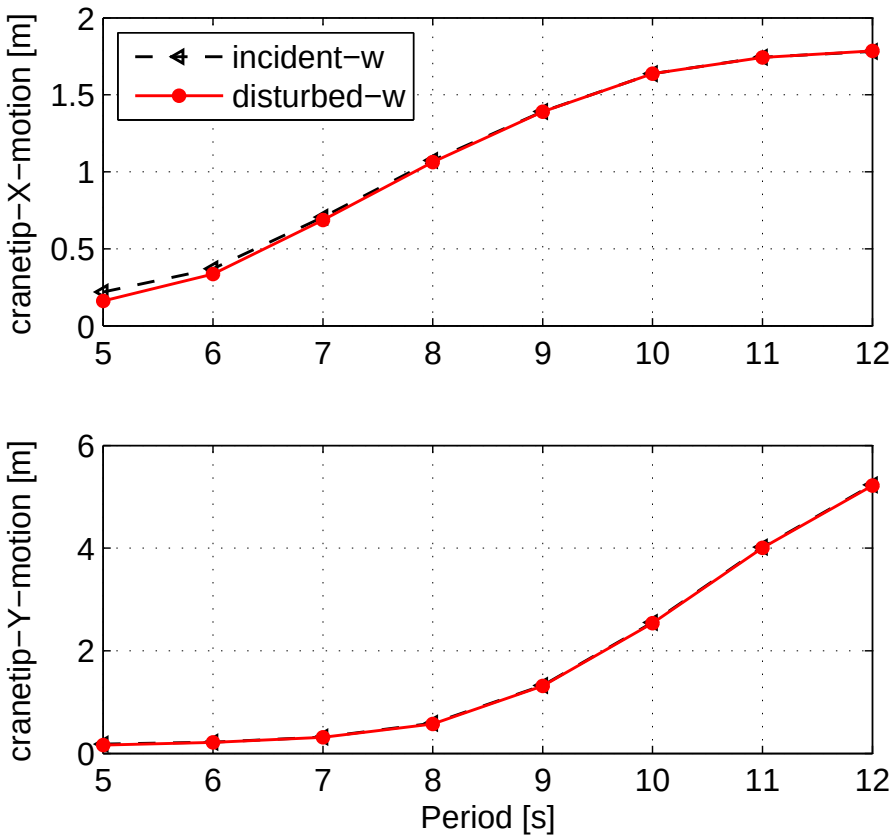

Fig. 18. Extreme crane tip motions in incident and disturbed waves ($H_s = 2.5\ m$, $Dir = 45\ deg$)

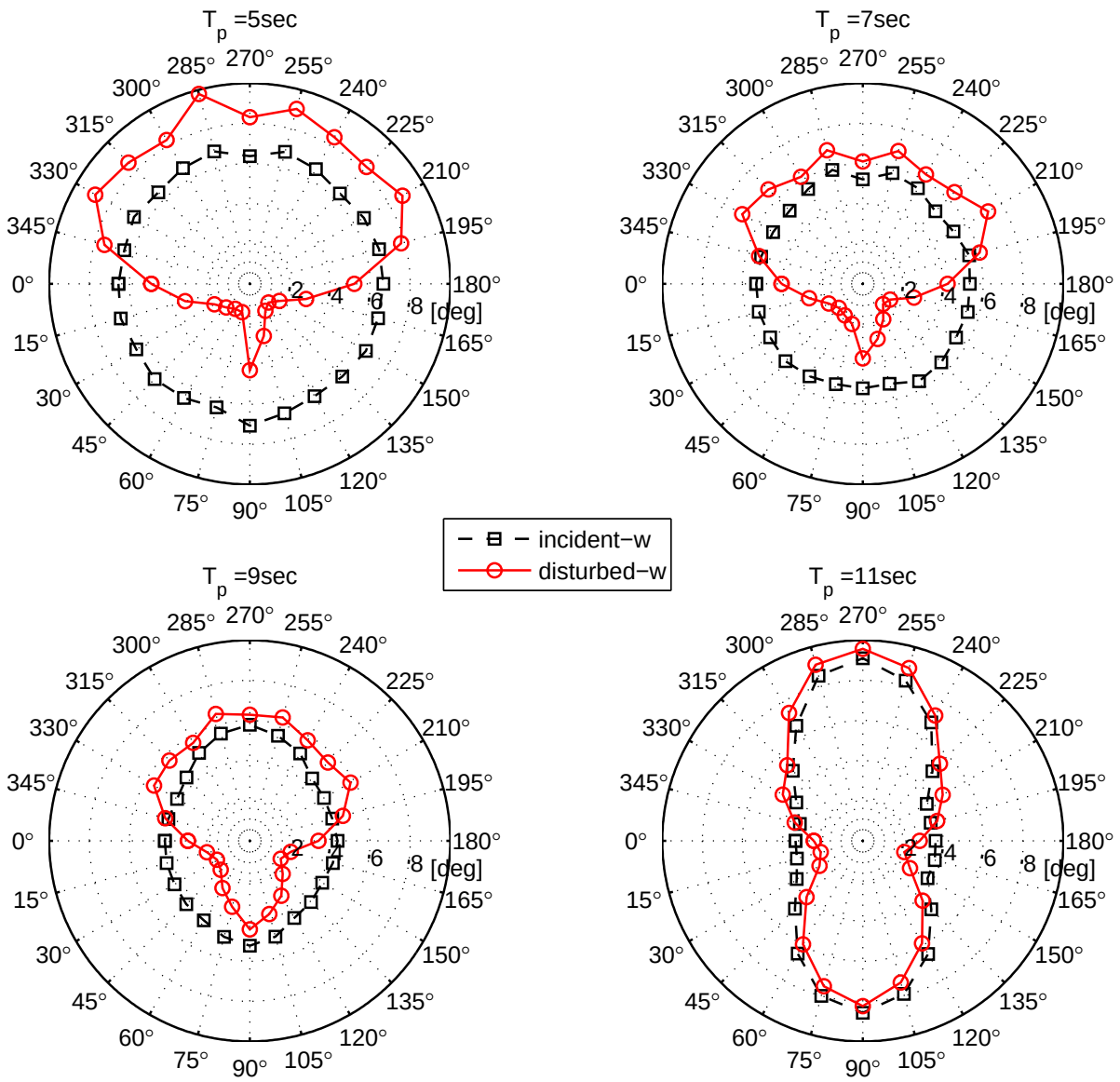

Fig. 19. Extreme rotations of monopile in incident and disturbed waves at different wave directions (H_s = 2.5 m)

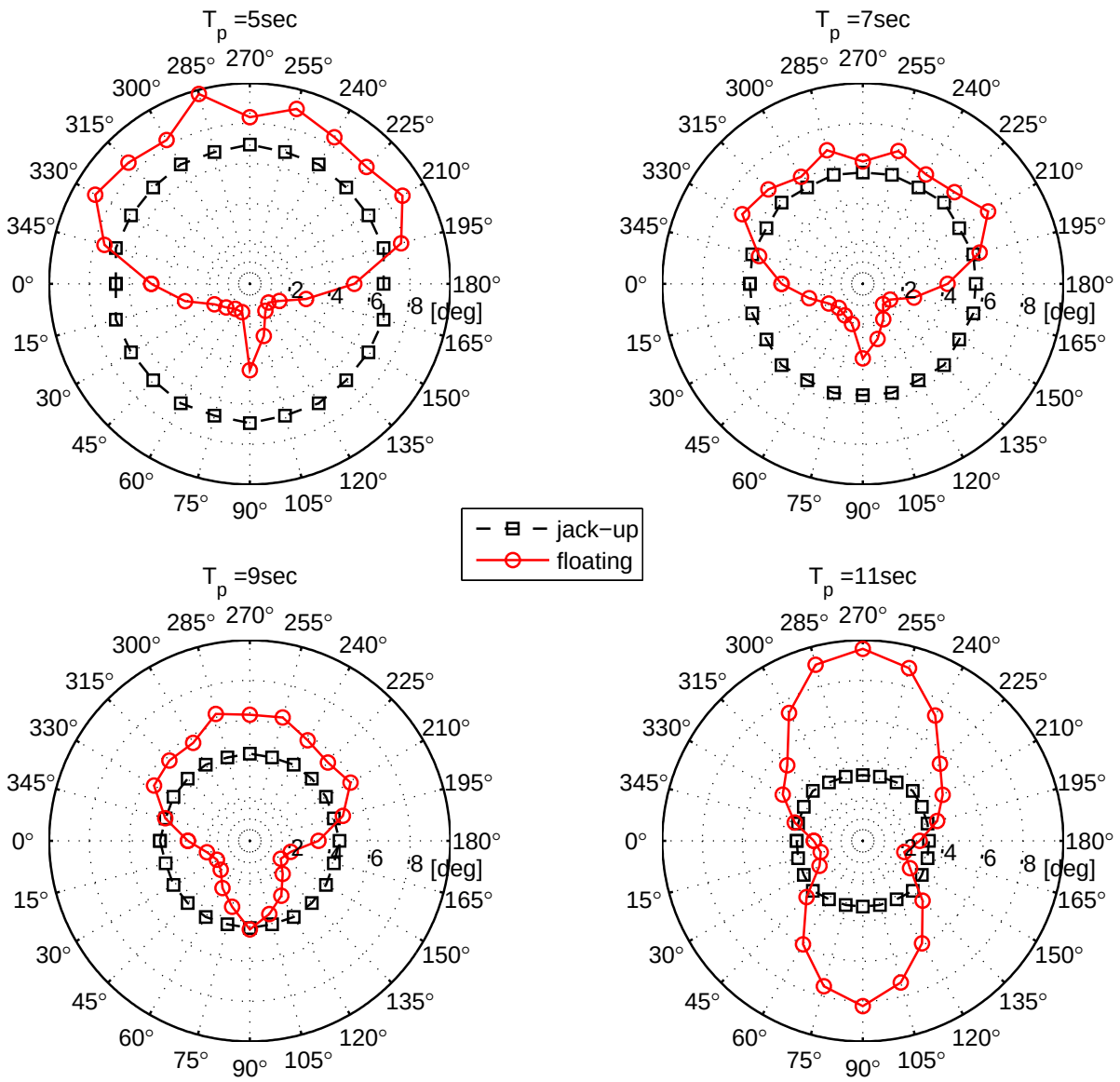

Fig. 20. Extreme monopile rotations by using jack-up and floating installation vessels at different wave directions ($H_s = 2.5\ m$)

9 TABLES

Table 1. Main parameters of the floating installation vessel and the monopile

Vessel			Monopile		
Length overall	$[m]$	183	Total mass	$[tons]$	500
Breadth	$[m]$	47	Length	$[m]$	60
Operational draught	$[m]$	12	Outer diameter	$[m]$	5.7
Displacement	$[tons]$	52000	Thickness	$[m]$	0.06

Table 2. Main parameters of the mechanical couplings

Lift wire			Gripper device		
EA/l_0	$[kN/m]$	7.00E+04	Stiffness	$[kN/m]$	4.00E+03
k_0	$[kN/m]$	5.00E+05	Damping	$[kNs/m]$	8.00E+02
Damping	$[kNs/m]$	1.40E+03			

Table 3. Eigenperiods and eigenvectors of vessel rigid body motions

Mode		1	2	3	4	5	6
Surge	$[m]$	-0.15	-0.06	0.00	0.00	**1.00**	0.00
Sway	$[m]$	0.00	0.00	0.06	**0.86**	0.00	**-0.79**
Heave	$[m]$	-0.29	**1.00**	0.00	0.00	0.00	0.00
Roll	$[deg]$	0.00	0.00	**1.00**	0.02	0.00	0.03
Pitch	$[deg]$	**1.00**	0.19	0.00	0.00	0.00	0.00
Yaw	$[deg]$	0.00	0.00	-0.01	**1.00**	0.00	**1.00**
Natural period	$[sec]$	9.44	10.65	13.54	93.89	99.98	105.36

Table 4. Eigenperiods and eigenvectors of monopile rigid body motions

Mode		1	2	3	4	5	6
Surge	$[m]$	0.03	-0.23	-0.23	0.39	-0.32	0.00
Sway	$[m]$	-0.03	-0.22	0.24	0.32	0.39	0.00
Heave	$[m]$	**1.00**	0.00	0.06	0.00	-0.03	0.00
Roll	$[deg]$	-0.28	**-0.96**	**1.00**	**-0.82**	**-1.00**	0.00
Pitch	$[deg]$	-0.29	**1.00**	**0.96**	**1.00**	**-0.82**	0.00
Yaw	$[deg]$	0.00	0.00	0.00	0.00	0.00	**1.00**
Natural period	$[sec]$	0.72	1.01	1.02	3.58	3.67	40.04

Table 5. Parameters for sensitivity study of wave point resolutions and environmental conditions

Sensitivity study case no.		1	2	3	4	5	6	7	8
Δx	$[m]$	0.5	2	4	8	–	–	–	–
Δy	$[m]$	0.5	2	4	8	–	–	–	–
Δz	$[m]$	2	2	2	2	0.5	0.5/2	2	4
Environmental condition no.		1	2	3	4				
T_p	$[sec]$	5	7	5	7				
Dir	$[deg]$	0	0	45	45				
λ	$[m]$	39	75	39	75				

Table 6. Differences in percentage between extreme responses in disturbed and incident waves

Dir $[deg]$	monopile rotation				lift wire tension				gripper force			
	5 sec	7 sec	9 sec	11 sec	5 sec	7 sec	9 sec	11 sec	5 sec	7 sec	9 sec	11 sec
0	-25.0	-23.7	-27.1	-27.2	-13.2	-8.0	-3.8	-0.9	-43.9	-35.4	-27.5	-27.2
15	-49.9	-48.4	-48.5	**-36.3**	-19.9	-11.1	**-5.0**	-0.7	-56.7	-50.2	-45.9	-40.9
30	-68.8	-63.2	**-56.4**	-34.5	-21.5	**-11.2**	-4.8	**-1.1**	-69.7	-62.0	-59.2	-48.6
45	-75.3	**-68.9**	-54.4	-17.1	**-22.1**	**-11.2**	-4.4	0.1	-71.5	-64.9	**-60.4**	**-51.6**
60	**-78.1**	-65.9	-40.6	-8.1	-21.2	-10.4	-3.6	0.7	-73.6	**-67.7**	-55.0	-47.0
75	-77.1	-60.0	-31.4	-6.3	-19.6	-8.5	-3.3	0.9	**-74.7**	-65.5	-56.3	-45.9
90	-39.1	-28.7	-15.6	-3.8	-10.1	-2.3	-0.7	1.0	-56.0	-51.1	-46.2	-35.7